Climate changes during the Late Glacial in southern Europe: new insights based on pollen and brGDGTs of Lake Matese in Italy

Mary Robles, Odile Peyron, Guillemette Ménot, Elisabetta Brugiapaglia, Sabine Wulf, Oona Appelt, Marion Blache, Boris Vannière, Lucas Dugerdil, Bruno Paura, et al.

Clim. Past, 19, 493–515, 2023
https://doi.org/10.5194/cp-19-493-2023

Climate of the Past
Open Access
EGU

Climate changes during the Late Glacial in southern Europe: new insights based on pollen and brGDGTs of Lake Matese in Italy

Mary Robles[1,2], Odile Peyron[2], Guillemette Ménot[3], Elisabetta Brugiapaglia[1], Sabine Wulf[4], Oona Appelt[5], Marion Blache[2], Boris Vannière[6,7], Lucas Dugerdil[2], Bruno Paura[1], Salomé Ansanay-Alex[3], Amy Cromartie[8], Laurent Charlet[9], Stephane Guédron[9], Jacques-Louis de Beaulieu[10], and Sébastien Joannin[2,3]

[1]Department of Agricultural, Environmental and Food Sciences, Univ. Molise, Campobasso, Italy
[2]ISEM, CNRS, IRD, EPHE, Univ. Montpellier, 34095 Montpellier, France
[3]LGL-TPE, ENS de Lyon, UCBL, UJM, CNRS, Univ. Lyon 1, 69007 Lyon, France
[4]School of the Environment, Geography and Geosciences, University of Portsmouth, Portsmouth, United Kingdom
[5]GFZ German Research Centre of Geosciences, Section 3.6, Helmholtz Centre Potsdam, Telegrafenberg, Potsdam, Germany
[6]Chrono-Environnement, CNRS, Univ. Bourgogne Franche-Comté, 25000 Besançon, France
[7]MSHE Ledoux, CNRS, Université Bourgogne Franche-Comté, 25000 Besançon, France
[8]Department of Anthropology, Cornell University, Ithaca, NY, USA
[9]ISTerre, IFSTTAR, CNRS, IRD, Univ. Grenoble Alpes, Univ. Savoie Mont Blanc, 38058 Grenoble, France
[10]IMBE, CNRS, IRD, Aix-Marseille Univ., Avignon Univ., 13545 Aix-en-Provence, France

Correspondence: Mary Robles (robles@cerege.fr) and Odile Peyron (odile.peyron@umontpellier.fr)

Received: 29 June 2022 – Discussion started: 28 July 2022
Revised: 24 October 2022 – Accepted: 8 November 2022 – Published: 23 February 2023

Abstract. The Late Glacial (14 700–11 700 cal BP) is a key climate period marked by rapid but contrasted changes in the Northern Hemisphere. Indeed, regional climate differences have been evidenced during the Late Glacial in Europe and the northern Mediterranean. However, past climate patterns are still debated since temperature and precipitation changes are poorly investigated towards the lower European latitudes. Lake Matese in southern Italy is a key site in the central Mediterranean to investigate climate patterns during the Late Glacial. This study aims to reconstruct climate changes and their impacts at Matese using a multi-proxy approach including magnetic susceptibility, geochemistry (XRF core scanning), pollen data and molecular biomarkers like branched glycerol dialkyl glycerol tetraethers (brGDGTs). Paleotemperatures and paleo-precipitation patterns are quantitatively inferred from pollen assemblages (multi-method approach: modern analogue technique, weighted averaging partial least-squares regression, random forest and boosted regression trees) and brGDGT calibrations. The results are compared to a latitudinal selection of regional climate reconstructions in Italy to better understand climate processes in Europe and in the circum-Mediterranean region. A warm Bølling–Allerød and a marked cold Younger Dryas are revealed in all climate reconstructions inferred from various proxies (chironomids, ostracods, speleothems, pollen, brGDGTs), showing no latitudinal differences in terms of temperatures across Italy. During the Bølling–Allerød, no significant changes in terms of precipitation are recorded; however, a contrasted pattern is visible during the Younger Dryas. Slightly wetter conditions are recorded south of 42° N, whereas dry conditions are recorded north of 42° N. During the Younger Dryas, cold conditions can be attributed to the southward position of North Atlantic sea ice and of the polar frontal jet stream, whereas the increase in precipitation in southern Italy seems to be linked to relocation of Atlantic storm tracks into the Mediterranean, induced by the Fennoscandian ice sheet and the North European Plain. By contrast, warm conditions during the Bølling–Allerød can be linked to the northward position of North Atlantic sea ice and of the polar frontal jet stream.

1 Introduction

In the Northern Hemisphere, the Late Glacial (ca. 14 700–11 700 cal BP) is a period of special climatic interest characterized by contrasted and rapid climate changes, associated with the successive steps of deglaciation and changes in atmospheric and ocean circulation patterns (e.g., Walker et al., 2012; Rehfeld et al., 2018). Following the cold Oldest Dryas (OD) period, the Bølling–Allerød (B/A) or Greenland Interstadial-1 (GI-1) began abruptly at 14 700 cal BP with warmer conditions. At 12 900–11 700 cal BP, the Younger Dryas (YD) or Greenland Stadial-1 (GS-1) was the last main millennial-scale cold event in Europe during the Late Glacial (Greenland ice core records; Rasmussen et al., 2014). The YD is characterized by extreme cold and relatively dry and windy climate conditions in northern and central Europe (Hepp et al., 2019). The climate became distinctly warmer at 11 700 cal BP with the onset of the Holocene Interglacial (Rasmussen et al., 2014). These rapid and marked climate oscillations have been observed in the Greenland ice core records (Rasmussen et al., 2014) and in Europe from various proxies such as pollen, oxygen isotopes, molecular biomarkers, beetles and chironomids (Coope and Lemdahl, 1995; Ammann et al., 2000; Peyron et al., 2005; Lotter et al., 2012; Millet et al., 2012; Blaga et al., 2013; Moreno et al., 2014; Heiri et al., 2015; Ponel et al., 2022; Duprat-Oualid et al., 2022).

Regional climate differences have been evidenced during the Late Glacial, and temperature trends in Europe and the Mediterranean region are still a matter of active research and debate. The chironomid-based synthesis of Heiri et al. (2014) suggests that temperature variations during the Late Glacial tend to be more pronounced in western Europe (British Isles, Norway) than in southwestern, central and southeastern Europe. This is particularly true for the Younger Dryas cooling, which is not well evidenced in the eastern and central parts of southern Europe (Heiri et al., 2014). These regional differences would be attributed to the changing position of North Atlantic sea ice and the polar frontal jet stream (Renssen and Isarin, 2001).

Diverging temperature trends are also reconstructed from different proxies during key periods of the Late Glacial. Studies suggest that (1) the OD was cooler than the YD in southern and central Europe in comparison to northern Europe ($\sim$ 1–3 °C; Heiri et al., 2014; Moreno et al., 2014), (2) the Allerød period was warmer than the Bølling period in southwestern Europe and the Mediterranean area ($\sim$ 1 °C; Moreno et al., 2014), and (3) temperatures were more contrasted during the B/A and YD in northwestern Europe in comparison to southern Europe (Renssen and Isarin, 2001; Moreno et al., 2014; Heiri et al., 2014). In contrast to temperature, the precipitation signal is poorly known in Europe during the Late Glacial because few proxies are available to quantitatively reconstruct precipitation change. Global climate models (GCMs) simulate significant hydrological changes during the B/A and contrasting north–south patterns during the YD (Renssen and Isarin, 2001; Rea et al., 2020). They simulate drier conditions in northern Europe and wetter conditions in southern Europe, i.e., in southern Italy, the Dinaric Alps and northern Turkey (Rea et al., 2020). Climate changes during the YD are attributed to a weak Atlantic meridional overturning circulation (AMOC) and a southward shift of the polar frontal jet stream (PFJS), linked to the elevation of the ice sheet, in particular the Laurentide ice sheet (Renssen and Isarin, 2001; Renssen et al., 2015; Rea et al., 2020). Rea et al. (2020) also explains the regional climate patterns in Europe via a relocation of Atlantic storm tracks along the western European margin and into the Mediterranean.

The understanding of climate processes in Europe and the Mediterranean during the Late Glacial still needs to be improved. The majority of climate reconstructions are focused on temperatures, and changes in precipitation remain elusive. The "key" junction area between northern and southern Europe and regional climatic patterns also need to be better defined. Moreover, the proxies used to reconstruct climate changes (e.g., Coleoptera, chironomids, pollen, ostracods, speleothems) can show differences in terms of amplitudes or patterns that are affected not only by temperature but also by precipitation or effective moisture (Moreno et al., 2014; Samartin et al., 2017). For these reasons, more reliable temperature reconstructions, especially from western Europe and the Mediterranean region, are required to test diverging trends during the Late Glacial. The proxies largely used to quantitatively reconstruct past climate changes are often a single-proxy approach (e.g., Heiri et al., 2015; Gandouin et al., 2016; Peyron et al., 2017; Marchegiano et al., 2020; Duprat-Oualid et al., 2022). Multiproxy approaches on the same sedimentary record, including independent climate proxies, are necessary to better understand the climate processes in Europe during the Late Glacial (Lotter et al., 2012; Ponel et al., 2022). Pollen-based reconstructions have the advantage of reconstructing temperatures, precipitation and seasonality; however, the climate signal can be perturbed by other factors such as CO_2 changes and human impact influencing vegetation development (Peyron et al., 2005). Over the last few decades, novel proxies based on molecular geochemistry have been developed and molecular biomarkers are being increasingly used to reconstruct temperatures and represent a complementary proxy for lake sediments (Castañeda and Schouten, 2011). In particular, branched glycerol dialkyl glycerol tetraethers (brGDGTs) are ubiquitous organic compounds synthesized by bacteria (Weijers et al., 2006), which have been useful for reconstructing environmental parameters. To date, the actual producers of brGDGTs remain elusive, although it is proposed they come from the phylum Acidobacteria (Weijers et al., 2009; Sinninghe Damsté et al., 2018). The relationships, however, between brGDGT distribution and environmental changes, in particular pH and temperature, are well established (Naafs et al., 2017a, b; Dearing Crampton-Flood et al.,

2020; Martínez-Sosa et al., 2021; Raberg et al., 2021). The degree of methylation of brGDGTs (MBT, methylation of branched GDGTs) varies depending on the mean annual air temperature (MAAT), and higher fractional abundances of hexa- (III) and penta-methylated (II) brGDGTs are recorded in colder environments (Weijers et al., 2007). Branched glycerol dialkyl glycerol tetraether (brGDGT) membrane lipids are increasingly used as a temperature proxy: in Europe, brGDGTs have been used to reconstruct the mid to late Holocene temperature changes in the Carpathians (Ramos-Román et al., 2022), the last 36 000 years in the southern Iberian Peninsula (Rodrigo-Gámiz et al., 2022), Holocene temperatures in France (Martin et al., 2020) and temperatures in the eastern Mediterranean over the last deglaciation (Sanchi et al., 2014; Stockhecke et al., 2021). The association in the same core between brGDGTs and other proxies such as pollen for climate reconstructions are still rare (Watson et al., 2018; Panagiotopoulos et al., 2020; Martin et al., 2020; Dugerdil et al., 2021a, b; Ramos-Román et al., 2022; Robles et al., 2022; Rodrigo-Gámiz et al., 2022), and no studies are yet available for the circum-Mediterranean region during the Late Glacial.

This study presents a high-resolution climate reconstruction for the Late Glacial period in southern central Europe, inferred from multi-proxy data of the Lake Matese sedimentary record (southern Italy). In detail, the aims of this study are to as follows:

1. to establish reliable and independent quantitative climate reconstructions based on molecular biomarkers (brGDGTs) and pollen data to help identify potential biases of currently used proxies and thus improve the reliability of each proxy-inferred climate record,

2. to compare these reconstructions with regional climate reconstructions and in the light of other southern European records,

3. to better understand the climate processes in Europe and Mediterranean during the Late Glacial period.

2 Study site

Lake Matese (41°24′33.3″ N, 14°24′22.1″ E, 1012 m a.s.l.) is located in the Caserta province in the Campania region, southern Italy, approximately 60 km north of the city of Naples and the active Campanian volcanoes (Vesuvius, Campi Flegrei, Ischia) (Fig. 1). The lake is situated in the Matese karst massif in the southern Apennines, which extends over 30 km from the NE to the SW and is composed of late Triassic–Miocene limestones and dolomites (Fiorillo and Doglioni, 2010). The present formation of the massif was the result of an extension by strike-slip faults during the Quaternary, and several strong earthquakes were recorded in the massif (Ferranti et al., 2015; Galli et al., 2017; Ferrarini et al., 2017; Valente et al., 2019). Lake Matese is the highest karst lake of Italy and is surrounded by the two highest peaks of the massif, Mount Miletto (2050 m a.s.l.) and Mount Gallinola (1923 m a.s.l.), which feed the lake with their snowmelt. Along the southern side of the lake, two sinkholes named the "Brecce" and "Scennerato" are present (Fiorillo and Pagnozzi, 2015). In the 1920s, hydraulic works were conducted to isolate the bottom of the lake and the main sinkholes by earthen dams (Fiorillo and Pagnozzi, 2015). The water level of the lake improved from 1007–1009 to 1012 m a.s.l. with a volume of 15 Mm^3 (Fiorillo and Pagnozzi, 2015). A part of the lake water is transported to the hydroelectric power station of Piedimonte Matese at the bottom of the mountain massif.

The Matese Mountains are characterized by a Mediterranean warm temperate, humid climate (Aucelli et al., 2013). The southeastern part of the massif, including Lake Matese, have the highest precipitation with a maximum of 2167 mm at Campitello Matese (1400 m a.s.l.) (Fiorillo and Pagnozzi, 2015). Lake Matese shows an annual precipitation of 1808 mm, with a maximum in November (∼ 290 mm) and December (∼ 260 mm) and a minimum in July (∼ 50 mm) (Fiorillo and Pagnozzi, 2015). The annual temperatures correspond to 9.3 °C, with a minimum in January (2 °C) and a maximum in July (19 °C) (Fiorillo and Pagnozzi, 2015).

The vegetation of the Matese massif is dominated by deciduous *Quercus* and *Ostrya carpinifolia*, while the highest altitudes at the northern flank also show an exposure of *Fagus sylvatica*, and the lower altitudes of the southern flank include Mediterranean taxa such as *Quercus ilex* (Taffetani et al., 2012; Carranza et al., 2012; Guarino et al., 2015). The hygrophilous vegetation at Lake Matese is distinguished by the presence of woody species (e.g., *Salix alba S. caprea*, *S. cinerea* subsp. *cinerea*, *Populus nigra*, *P. alba*), helophyte species (e.g., *Phragmites australis*, *Schoenoplectus lacustris*, *Typha angustifolia*, *T. latifolia*) and hydrophyte species (*Myriophyllum spicatum*, *Persicaria amphibia*).

3 Material and methods

3.1 Coring retrieval

Coring of Lake Matese was performed in July 2019 in the southwestern part of the lake (41°24′33.3″ N, 14°24′22.1″ E, 1012 m a.s.l.). The core occurred on a floating raft composed of *Salix* spp. and *Phragmites* spp., naturally present in the eastern part of the lake. Three parallel cores (cores A, B and C) were taken with a 1 m Russian corer with a chamber diameter of 6.3 cm. The composite core, measuring 535 cm, was constructed from sections of parallel cores and is based on the lithology and XRF data.

Figure 1. Location of the Lake Matese and Late Glacial paleoclimate records: Hölloch (Li et al., 2021), Maloja Riegel (Heiri et al., 2014), Lake di Lavarone (Heiri et al., 2014), Lake Piccolo di Avigliana (Larocque and Finsinger, 2008), Lake Gemini (Samartin et al., 2017), Lake Verdarolo (Samartin et al., 2017), Corchia cave (Regattieri et al., 2014), Lake Trasimeno (Marchegiano et al., 2020), Lake Grande di Monticchio (Allen et al., 2002), MD90-917 (Sicre et al., 2013; Combourieu-Nebout et al., 2013), BS7938 (Sbaffi et al., 2004), MD04-2797 (Sicre et al., 2013; Desprat et al., 2013). The dotted line indicates 42° N. The locations of active Campanian volcanoes (Vesuvius, Campi Flegrei, Ischia) are also marked.

3.2 Chronology and age–depth model

Several methods have been used to build the chronology of the core, including radiocarbon dating and tephrochronology. The regional pollen stratigraphy is used to validate this age–depth model. A total of 12 accelerator mass spectrometry (AMS) ^{14}C dates were measured at the Poznań Radiocarbon Laboratory and at the Radiocarbon Dating Center in Lyon. Plant macrofossils (plant fibers, wood) and charcoal were selected for four samples, and bulk sediment was used for eight samples according to the sediment type. Radiocarbon ages were calibrated in calibrated years BP using the Calib 8.2 software with the IntCal20 calibration curve (Reimer et al., 2020).

Visible tephra layers and cryptotephra layers, detected by magnetic susceptibility and XRF core scanning data, were subsampled and processed for geochemical analysis. Cryptotephra were extracted using H_2O_2 and HCl to remove organic matter and carbonates and sieved at 20 and 100 µm, and volcanic glass shards were embedded in resin, sectioned and polished for electron probe microanalysis. A JEOL-JXA8230 probe at the Helmholtz Centre Potsdam (Germany) was used with a 15 kV accelerating voltage, 10 nA beam current and a 15 µm beam size. Analytical count times were 20 s for all elements except for K and Na, measured first at 10 s. International glass standards, such as the Max Planck Institute (MPI-glasses) ATHO-G, StHs6/80 and GOR-132 (Jochum et al., 2006) and the natural Lipari obsidian (Hunt and Hill, 1996; Kuehn et al., 2011), were measured prior to sample analysis for data quality assurance. Geochemical glass data of the Matese tephra are normalized on an anhydrous, volatile-free basis and compared with published tephra glass datasets (Wulf et al., 2008; Smith et al., 2011; Tomlinson et al., 2012).

The age–depth model based on one radiocarbon date and correlated tephra ages was constructed using an interpolated linear curve with the R *Clam* program using 95 % confidence intervals (Blaauw, 2010). In order to validate the age–depth models, the pollen stratigraphy of the regional sites was compared with pollen data at Matese. The pollen stratigraphy of Pavullo nel Frignano (Vescovi et al., 2010) and lakes Accesa (Drescher-Schneider et al., 2007), Albano (Mercuri et al., 2002), Mezzano (Sadori, 2018), Monticchio (Allen et al., 2002) and Trifoglietti (De Beaulieu et al., 2017) were used to identify the OD–B/A, B/A–YD and YD–Holocene transitions. We used the median age for each transition.

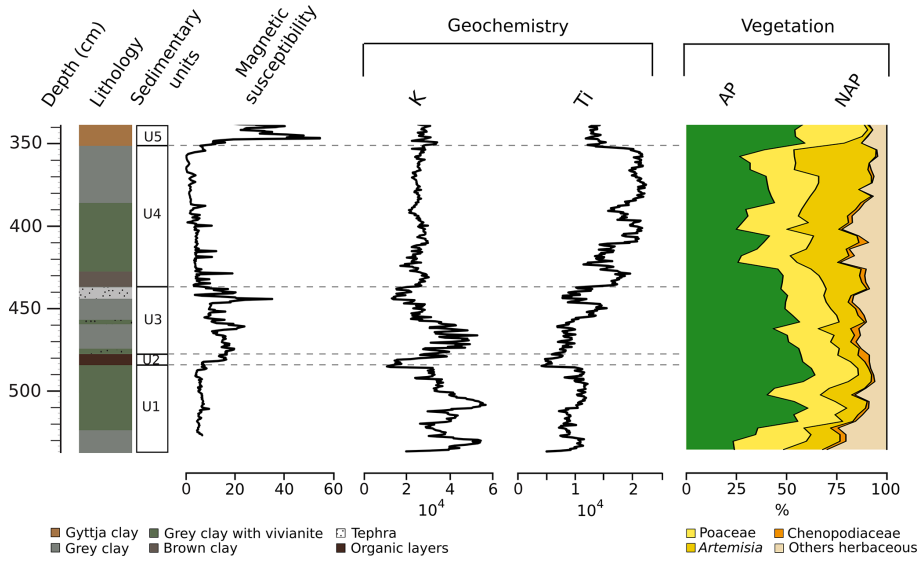

Figure 2. Sediment lithology, magnetic susceptibility, geochemical data and selected terrestrial pollen taxa at Matese. Arboreal pollen (AP; green) and non-arboreal pollen (NAP; yellow and orange) are expressed in percentages of total terrestrial pollen.

3.3 Magnetic susceptibility and geochemistry

Magnetic susceptibility (MS) was measured with a MS2E1 surface-scanning sensor from Bartington Instruments on a Geotek Multi-Sensor Core logger based at the Chrono-Environment laboratory (UMR CNRS – University of Franche-Comté). An interval of 3 or 5 mm was applied depending on the type of sediment.

Geochemical analyses were performed at high resolution by X-ray fluorescence (XRF) with an AVAATECH core scanner at the EDYTEM laboratory (University Savoie Mont Blanc). A continuous 5 mm step measurement was applied with a run at 10 kV and 0.1 mA for 15 s to detect lightweight elements, such as Al, Si, K, Ca, Ti, Mn and Fe, and a second run was performed at 30 kV and 0.15 mA for 20 s to detect Br, Rb, Sr and Zr. The XRF core scanning provides an estimate of the geochemical composition, and the results are semi-quantitative and expressed as peak intensity counts, i.e., counts per second (cps).

3.4 Pollen analyses

A total of 56 samples from the Matese core were collected at 4 or 6 cm resolution for pollen analysis. For each sample, 1 cm^3 of sediment was processed and three *Lycopodium* tablets were added to estimate pollen concentration. Samples were treated following the standard procedure (Faegri et al., 1989; Moore et al., 1991) including HCl, potassium hydroxide (KOH), sieving, acetolysis and hydrofluoric acid (HF).The pollen concentrates were analyzed with a Leica DM1000 LED microscope at a standard magnification of 400×. Pollen taxa were identified using photo atlases (Reille, 1998; Van Geel, 2002; Beug, 2004) and a modern reference collection (ISEM, University of Montpellier). Each slide was counted with a minimum of 300 terrestrial pollen grains, excluding aquatic plants such as Cyperaceae, aquatic taxa and fern spores. A simplified pollen diagram was constructed (Fig. 2) with the R package *Rioja* (Juggins and Juggins, 2020). This study presents the main pollen taxa and is not focused on variations of individual species.

3.5 Pollen-inferred climate reconstruction

A multi-method approach was used to reconstruct climate parameters from pollen data with greater reliability than reconstructions based on a single climate reconstruction method (Peyron et al., 2005, 2011, 2013; Salonen et al., 2019). We have selected the modern analog technique (MAT; Guiot, 1990), weighted averaging partial least-squares regression (WAPLS; ter Braak and van Dam, 1989; ter Braak and Juggins, 1993), and the most recent machine-learning methods: random forest (RF; Breiman, 2001; Prasad et al., 2006) and boosted regression trees (BRT; De'ath, 2007; Elith et al., 2008).

The MAT is an assemblage approach based on the measure of the degree of dissimilarity (squared chord distance) between fossil and modern pollen assemblages (Guiot, 1990). Fossil pollen assemblages are compared to a set of modern assemblages (modern dataset), and each one is associated with climate estimates. The closest modern samples are retained and averaged to estimate past climate conditions (annual and seasonal temperature and precipitation). WAPLS is a nonlinear regression technique that models the relationships between the climate parameters and the pollen taxa from a modern pollen dataset, before applying these relationships to fossil pollen assemblages (ter Braak and van Dam,

1989; ter Braak and Juggins, 1993). WAPLS and MAT methods are applied with the R package *Rioja* (Juggins and Juggins, 2020). RF and BRT, based on machine learning, utilize regression trees developed with ecological data and have been used recently to reconstruct paleoclimatic changes (Salonen et al., 2019; Robles et al., 2022). These classification trees are used to partition the data by separating the pollen assemblages based on the relative pollen percentages. RF is based on a large number of regression trees, each tree being estimated from a randomized ensemble of different subsets of the modern pollen dataset by bootstrapping (Breiman, 2001; Prasad et al., 2006). Finally, the RF prediction is applied to the fossil pollen record. BRT is also based on regression trees (De'ath, 2007; Elith et al., 2008); it differs from RF in the definition of the random modern datasets. In RF, each sample gets the same probability of being selected, while in BRT the samples that were insufficiently described in the previous tree get a higher probability of being selected. This approach is called "boosting" and increases the performance of the model over the elements that are least well predicted (Breiman, 2001; Prasad et al., 2006; De'ath, 2007; Elith et al., 2008). RF is applied with the R package *randomForest* (Liaw and Wiener, 2002), and BRT is applied with the R package *dismo* (Hijmans et al., 2021).

The modern pollen dataset ($n = 3373$ sites) used for the calibration of the methods is based on the large Eurasian and Mediterranean dataset compiled by Peyron et al. (2013, 2017) and completed by Dugerdil et al. (2021a) and Robles et al. (2022). In our study, we added pollen data of 92 surface lake sediments from Italy (Finsinger et al., 2007) and 15 moss polsters from the Matese massif (Robles, 2022). Following this, a biome constraint (Guiot et al., 1993), based on the pollen plant functional type method and following the biomization procedure (Prentice et al., 1996; Peyron et al., 1998) was applied to modern and fossil pollen samples. The modern pollen dataset finally selected for the calibration of the different methods contains 1018 samples belonging to three biomes depicted in the fossil core: "warm mixed forest" (WAMX), "temperate deciduous" (TEDE) and "cold steppe" (COST). The performance of each method and calibration training were statistically tested (for more details, see Dugerdil et al., 2021a) to determine if modern samples are suitable for quantitative climate reconstructions. The root-mean-square error (RMSE) and the R^2 are presented in Table S1 in the Supplement. Five climate parameters were reconstructed: mean annual air temperature (MAAT), mean temperature of the warmest month (MTWA), mean temperature of the coldest month (MTCO), mean annual precipitation (PANN) and winter precipitation (P_{winter} = December, January and February). For each climate parameter, the methods fitting with the higher R^2 and the lower RMSE were selected. Cyperaceae and ferns in the Matese record have been excluded because they are associated with local dynamics.

3.6 BrGDGT analyses

A total of 56 samples from the Matese core (4 or 6 cm resolution) were used for GDGT analysis (same as for pollen analysis). The samples were freeze-dried, powdered and subsampled (1 g for clay and 0.4 g for gyttja). Lipids were extracted from the sediment using a microwave oven (MARS 6; CEM) with dichloromethane : methanol (3 : 1). Following this, the internal standard was added (C_{46} GDGT, Huguet et al., 2006). The total lipid extracts were separated into apolar and polar fractions using a silica solid-phase extraction (SPE) cartridge with hexane : dichloromethane (DCM) (1 : 1) and DCM : MeOH (1 : 1). The polar fractions containing brGDGTs were analyzed using high-performance liquid chromatography mass spectrometry (HPLC-APCI-MS, Agilent 1200) with detection via selective ion monitoring (SIM) of m/z 1050, 1048, 1046, 1036, 1034, 1032, 1022, 1020 and 1018 in the LGL-TPE of ENS Lyon (Hopmans et al., 2016; Davtian et al., 2018). GDGT concentrations were calculated based on the internal standard (C_{46} GDGT, Huguet et al., 2006). The analytic reproducibility was assessed by regularly processing a lab-internal sediment sample (Vaux Marsh; 45°57′21.1″ N, 5°35′32.42″ E). Analytical precision is based on duplicate injections of one sample of each Matese core lithological type ($n = 4$). Respective analytical 1-sigma standard deviations are then applied to each measurement within one lithology.

3.7 GDGT-based annual temperature reconstruction

The proportion of tetra- (I), penta- (II) and hexamethylated (III) brGDGTs includes the fractional abundances of the 5-methyl (X), 6-methyl (X') and 7-methyl ($X7$) brGDGTs (Ding et al., 2016). The CBT (cyclization ratio of branched tetraethers) and MBT indexes were defined by Weijers et al. (2007), and the $\text{MBT}'_{5\text{me}}$, only based on the 5-methyl brGDGTs, were defined by De Jonge et al. (2014). The mean annual air temperature (MAAT) was reconstructed with global (Sun et al., 2011) and East African (Russell et al., 2018) lacustrine calibrations. The mean temperature of months above freezing (MAF) was reconstructed with a lacustrine calibration based on Bayesian statistics (Martínez-Sosa et al., 2021; https://github.com/jesstierney/BayMBT, last access: June 2022) and global lacustrine calibrations with revised compound fractional abundances based on methylation and cyclization numbers and methylation position (Raberg et al., 2021). Synthesis of the formulae for the main brGDGT indices are presented in Table 1. Modern MAAT and MAF of the Lake Matese correspond to 9.3 °C.

The analytic reproducibility corresponds to ±0.040 for CBT, ±0.0167 for MBT, ±0.0206 for $\text{MBT}'_{5\text{me}}$, ±0.8566 °C for MAAT developed by Sun et al. (2011), ±0.6672 °C for MAAT developed by Russell et al. (2018), and ±0.5403 and ±1.1258 °C for MAF_{Meth} and MAF_{Full} developed by Raberg et al. (2021), respectively.

Table 1. Synthesis of the formulae for the main brGDGT indices. For a full explanation of MAF_{Meth} and MAF_{Full}, see Raberg et al. (2021). For more information about the Bayesian statistics, see Martínez-Sosa et al. (2021) and references therein.

Index	Formula	Reference
% tetra	$\frac{Ia+Ib+Ic}{\Sigma brGDGTs}$	Ding et al. (2016)
% penta	$\frac{IIa+IIa'+IIa_7+IIb+IIb'+IIb_7+IIc+IIc'+IIc_7}{\Sigma brGDGTs}$	Ding et al. (2016)
% hexa	$\frac{IIIa+IIIa'+IIIa_7+IIIb+IIIb'+IIIb_7+IIIc+IIIc'+IIIc_7}{\Sigma brGDGTs}$	Ding et al. (2016)
CBT	$-\log \frac{Ib+IIb}{Ia+IIa}$	Weijers et al. (2007)
MBT	$\frac{Ia+Ib+Ic}{\Sigma brGDGTs}$	Weijers et al. (2007)
MBT'_{5me}	$\frac{Ia+Ib+Ic}{Ia+Ib+Ic+IIa+IIb+IIc+IIIa}$	De Jonge et al. (2014)
MAAT (°C)	$3.949 - 5.593 \times CBT + 38.213 \times MBT$ $\left(n = 100,\ R^2 = 0.73,\ RMSE = 4.27\,°C\right)$	Sun et al. (2011)
MAAT (°C)	$-1.21 + 32.42 \times MBT'_{5me}$ $\left(n = 65,\ R^2 = 0.92,\ RMSE = 2.44\,°C\right)$	Russell et al. (2018)
MAF_{Meth} (°C)	$92.9 + 63.84 \times fIb^2_{Meth} - 130.51 \times fIb_{Meth}$ $-28.77 \times fIIa^2_{Meth} - 72.28 \times fIIb^2_{Meth}$ $-5.88 \times fIIc^2_{Meth} + 20.89 \times fIIIa^2_{Meth}$ $-40.54 \times fIIIa_{Meth} - 80.47 \times fIIIb_{Meth}$ $\left(n = 182,\ R^2 = 0.90,\ RMSE = 2.14\,°C\right)$	Raberg et al. (2021)
MAF_{Full} (°C)	$-8.06 + 37.52 \times fIa_{Full} - 266.83 \times fIb^2_{Full}$ $+133.42 \times fIb_{Full} + 100.85 \times fIIa'^2_{Full}$ $+58.15 \times fIIIa'^2_{Full} + 12.79 \times fIIIa_{Full}$ $\left(n = 182,\ R^2 = 0.91,\ RMSE = 1.97\,°C\right)$	Raberg et al. (2021)
MAF (°C)	Equation from the Bayesian model: $MBT'_{5me} = 0.030(\pm0.001)MAF + 0.075(\pm0.012)$ $\left(R^2 = 0.82,\ RMSE = 2.9\,°C\right)$	Martínez-Sosa et al. (2021)

4 Results

4.1 Lithology, magnetic susceptibility, XRF and pollen

The lithology of the Matese core (Fig. 2) is mainly composed of gray clay sediment with vivianite from the base to 350 cm, interrupted by an organic layer between 477 and 484 cm (sedimentary Unit 2) and a macroscopically visible tephra layer (Fig. 2) between 476 and 437 cm (sedimentary Unit 3). This part contains few plant fibers, which are essentially vertically oriented in the core. From 349 to 320 cm, the lithology is formed by a mix of clay sediment and gyttja (sedimentary Unit 5). This part is mostly composed of roots and fine rootlets.

Magnetic susceptibility (MS) and potassium (K) peaks of XRF core scanning are used to detect tephra layers (Fig. 2). MS and K contents show increased values at 516–502, 482–437 and 366–338 cm, which correspond to the deposition of tephra material (macroscopic visible tephra and cryptotephra of primary and secondary deposition). Small peaks are also visible in MS between 430 and 360 cm, but they are not associated with any observed tephra. Potassium content is also marked by an increase between 536 and 526 cm, which corresponds to tephra of primary deposition. Titanium (Ti) content, in contrast, is representative for terrigenous input, which is prevailing in sedimentary Unit 4 (Fig. 2).

The main pollen taxa diagram (Fig. 2) shows the dominance of herbaceous taxa (Poaceae, *Artemisia*) and a small proportion of arboreal taxa at the base of the sequence. From 520 to 425 cm, the period is marked by three expansion phases of arboreal taxa, followed between 438 and 354 cm by a large increase in *Artemisia* and a drop in AP taxa starting at 422 cm. Finally, from 354 to 338 cm AP and Poaceae increase, whereas *Artemisia* significantly decline.

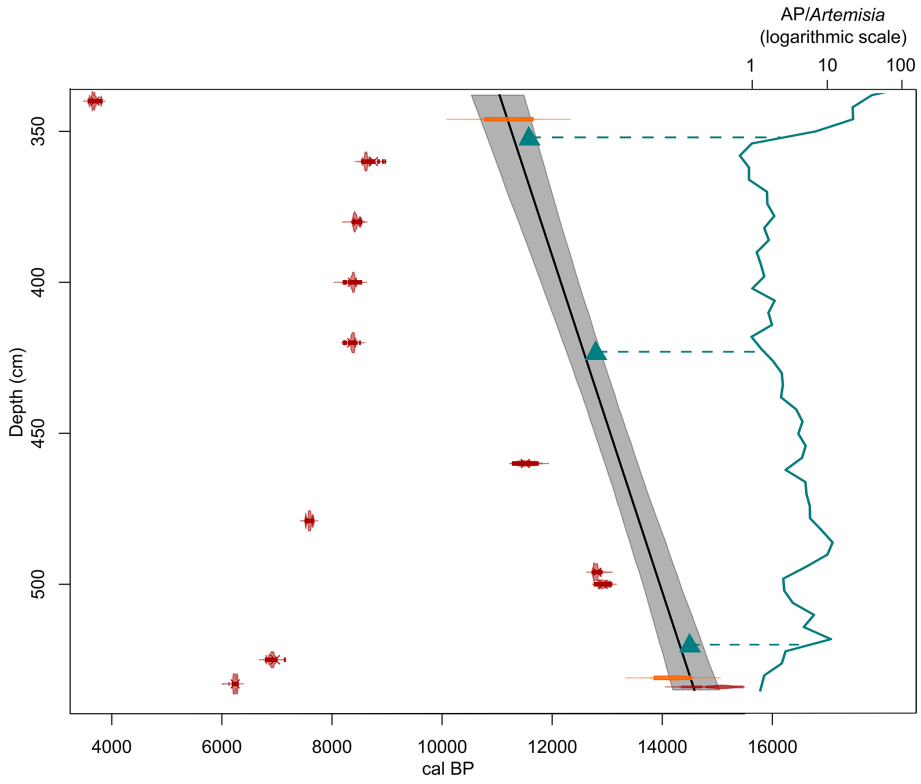

Figure 3. Age–depth model based on calibrated AMS radiocarbon dates (red points; Table 3) and tephra ages (orange points; Table 2). The gray band is the 95 % confidence interval. Blue triangles are the median ages of the vegetation transition compiled with the regional pollen stratigraphy. This pollen stratigraphy includes the sites of Pavullo nel Frignano (Vescovi et al., 2010), Accesa (Drescher-Schneider et al., 2007), Albano (Mercuri et al., 2002), Mezzano (Sadori, 2018), Monticchio (Allen et al., 2002) and Trifoglietti (De Beaulieu et al., 2017). The AP/*Artemisia* ratio (blue line) is expressed on a logarithmic scale. AP stands for arboreal pollen.

Table 2. Tephra samples from Matese cores (MC) and correlation with tephra samples from Lake Grande di Monticchio (Wulf et al., 2008) and proximal eruptive sources.

Sample ID	Depth MC (cm)	Tephra Monticchio	Eruption	Age (cal BP)	Age reference
C1 96–97	346	TM-6-2	Casale	11 210 ± 224	Wulf et al. (2008)
A5 75–77 C3 83–84 B5 95–96	475 (reworked) 510 (reworked) 530	TM-8	Neapolitan Yellow Tuff (NYT)	14 194 ± 172	Bronk Ramsey et al. (2015)

4.2 Age–depth model

The age–depth model is based on ^{14}C dates and tephrochronology, and then pollen stratigraphy was used to validate the age–depth model (Fig. 3). Based on their typical phono-trachytic and bimodal tephri-phonolitic to trachytic major element glass composition, Matese tephra at 530 and 346 cm depth can be correlated with distal Monticchio tephra samples TM-8 and TM-6-2, respectively (Fig. 4; Table 2). Tephra TM-8 has been correlated with the Neapolitan Yellow Tuff (NYT) eruption (Wulf et al., 2004), which has an age of 14 194 ± 172 cal BP (Bronk Ramsey et al., 2015). The tephra layer at 530 cm corresponds to the primary deposition and secondary deposition of remobilized tephra samples that were identified at 510 and 475 cm. TM-6-2 is most likely derived from the early Holocene Casale eruption from Campi Flegrei (Smith et al., 2011), which is varve dated at Monticchio at 11 210 ± 224 cal BP (Wulf et al., 2008). The tephra layer at 346 cm corresponds to a primary deposition.

The ages obtained with the regional pollen stratigraphy show an OD–B/A transition at 14 500 ± 93.7 cal BP, a B/A–YD transition at 12 800 ± 57.7 cal BP and a YD–Holocene transition at 11 575 ± 103.1 cal BP (Allen et al., 2002; Mercuri et al., 2002; Drescher-Schneider et al., 2007; Vescovi

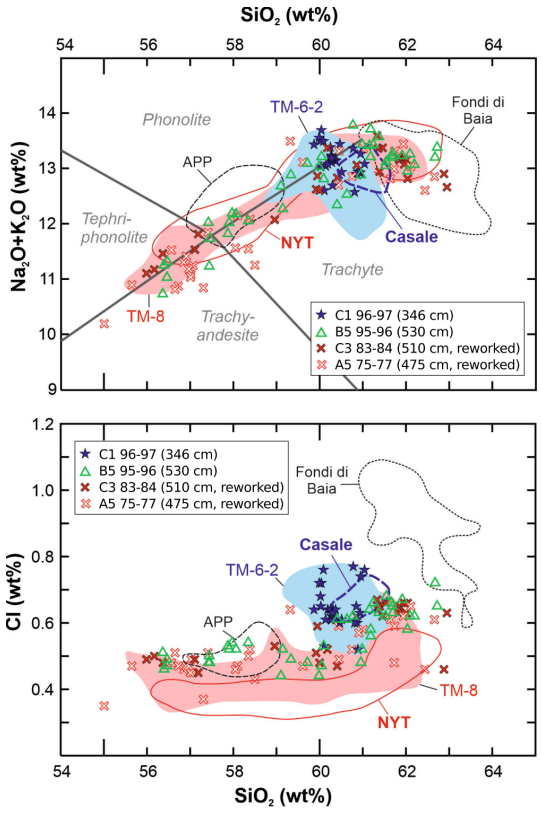

Figure 4. Bivariate plot of selected major elements (SiO_2 vs. total alkalis and SiO_2 vs. Cl) of the Matese tephra and potential proximal and Monticchio tephra correlatives. Data are taken from TM-6-2 (Monticchio, Wulf et al., 2008; this study), TM-8 (Monticchio, Tomlinson et al., 2012; this study), Casale in Fondi di Baia (proximal; Smith et al., 2011), and Agnano Pomici Principali (APP) and Neapolitan Yellow Tuff (NYT, proximal; Tomlinson et al., 2012).

et al., 2010; De Beaulieu et al., 2017; Sadori, 2018). Pollen stratigraphy of the regional sites was compared with pollen data at Matese, and the ages obtained show a good correspondence with the ages of tephra samples but a poor correspondence with the ^{14}C dates. Therefore, most of the ^{14}C dates (Table 3) are not included in the age–depth model (except the date at the base of the core). The organic matter extracted from sediment was essentially composed of rootlets, which explains the rejuvenation of the ^{14}C ages.

4.3 Pollen-inferred climate reconstructions

Pollen-inferred climate reconstructions at Matese show similar trends for all methods (Fig. 5). The MAT and the BRT methods show higher sample-to-sample variability than the WAPLS, and RF appears to be the less sensitive method. Statistical results of the model performance (Table S1) show the better values for R^2 and RMSE for the BRT method (all climatic parameters).

Temperature trends show two cold periods (phases 1 and 3) and two warm periods (phases 2 and 4). The reconstructed values (MAAT and MTWA) during the warm periods are close to modern values, whereas the values of MTCO are lower than the modern values. Annual precipitation (PANN) shows few variations, and the values of PANN and P_{winter} are lower than modern values with all methods. Phase 1 (535–530 cm; 14 600–14 500 cal BP) is characterized by cold conditions and low precipitation during winter. Phase 2 (530–436 cm; 14 500–12 800 cal BP) is a warm period characterized by strong warming and punctuated by three colder events at 14 000, 13 500–13 350 and 13 000 cal BP. Mean annual precipitation shows little variation, whereas P_{winter} shows higher values than during phase 1. Phase 3 (436–367 cm; 12 800–11 570 cal BP) is a strong event marked by cold conditions, a slight decline in P_{winter} and few changes for PANN. At the transition with phase 4, a significant decrease in the precipitation parameters is recorded. Phase 4 (367–338 cm; 11 570–11 000 cal BP) is characterized by a well-marked temperature increase (MAAT and MTCO) associated with wet conditions (hydrological parameters reach their maximum value).

4.4 BrGDGT-inferred climate reconstruction

4.4.1 Concentration and distribution of brGDGTs

The total concentration of brGDGTs ranges between 0.06 and 8.63 $\mu g\,g^{-1}$ dry sediment. The fractional abundances of brGDGTs (Fig. 6a) show a dominance of penta-methylated brGDGTs (II, 46 %), especially brGDGT II*a* (23 %), brGDGTs II*a*′ (7 %) and brGDGTs II*b* (6 %). The relative abundance of tetra-methylated brGDGTs (I, 33 %) is mainly explained by brGDGT I*a* (20 %) and brGDGTs I*b* (9 %). The relative abundance of hexa-methylated brGDGTs (III, 21 %) is mainly explained by brGDGT III*a* (11 %) and brGDGTs III*a*′ (6 %). The relative abundances of tetra-, penta- and hexa-methylated brGDGTs of the Matese core are compared to global datasets (Fig. 6b). Sediment samples of the Matese core show a good correspondence with global lake and soil samples, except for some samples from sedimentary Unit 1 and Unit 5. Samples of sedimentary Unit 5, characterized by a mix of clay and gyttja, are more similar to global soil and peat samples.

4.4.2 Indices of brGDGTs

The relative abundance of tetra-, penta- and hexa-methylated brGDGTs changes along the Matese core (Fig. 7). The fractional abundance shows a dominance of penta-methylated brGDGTs except at 518 cm depth and during the last phase (phase 4). The fractional abundance of hexa-methylated brGDGTs shows higher values between 535–502 and 490–466 cm and becomes dominant at 486 cm. The fractional abundance of tetra-methylated brGDGTs shows higher val-

Table 3. AMS radiocarbon dates (Radiocarbon Laboratory, Poznań), calibrated median ages and the 2σ range of calibration from Matese cores (MC).

Sample ID	Depth MC (cm)	Lab code	Material	AMS ^{14}C age (BP)	Age (cal BP) (2σ)	Median age (cal BP)
A4 40–41	340	Poz-128971	Bulk	3425 ± 30	3573–3822	3668
A4 60–61	360	Poz-138111	Bulk	7850 ± 40	8540–8968	8631
A4 80–81	380	Poz-138112	Bulk	7640 ± 50	8370–8541	8432
B4 50–51	400	Poz-128972	Bulk	7580 ± 60	8206–8519	8385
A5 20–21	420	Poz-138113	Bulk	7570 ± 50	8206–8512	8379
A5 60–61	460	Poz-128976	Bulk	$10\,020 \pm 50$	11 280–11 743	11 519
A6 52–53	479	Poz-119283	Plant fibers, wood fragments, charcoals	6730 ± 40	7513–7669	7596
A5 96–97	496	Poz-137155	Wood fragments	$10\,870 \pm 60$	12 728–12 903	12 799
B5 64–65	500	Poz-128973	Bulk	$11\,000 \pm 60$	12 769–13 078	12 925
A6 98–99	525	Poz-119284	Plant fibers	6060 ± 35	6795–7147	6912
B5 97–98	533	60 747	Plant fibers	5430 ± 30	6190–6295	6236
B5 98–99	534	Poz-128975	Bulk	$12\,650 \pm 130$	14 331–15 477	15 027

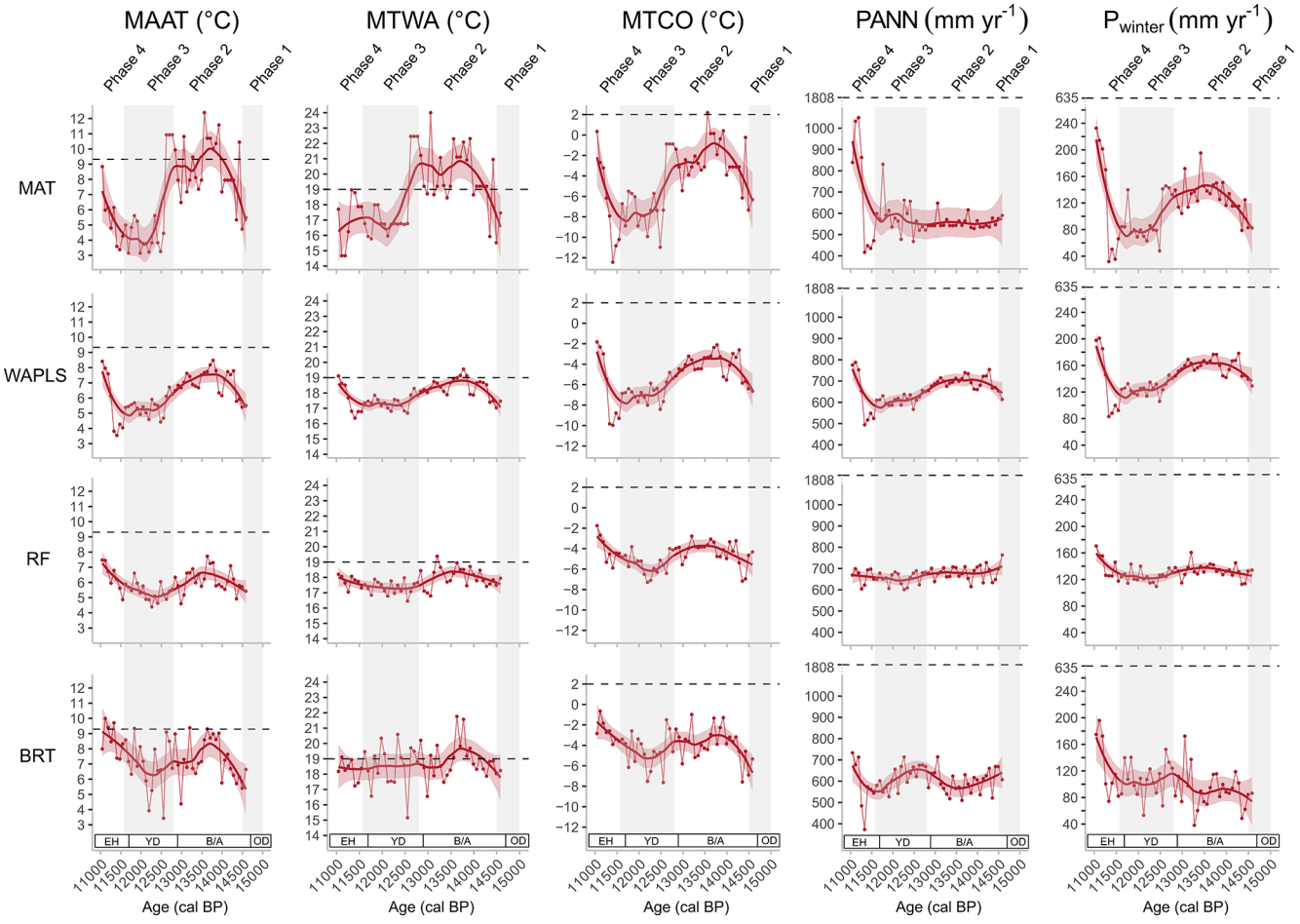

Figure 5. Lake Matese pollen-inferred climate reconstruction based on four methods of measuring against age: MAT (modern analogue technique), WAPLS (weighted averaging partial least-squares regression), RF (random forest) and BRT (boosted regression trees). Large lines correspond to LOESS smoothed curves, shaded areas correspond to the 95 % confidence interval and dashed lines correspond to modern climate values of Lake Matese. MAAT stands for mean annual air temperature. MTWA stands for mean temperature of the warmest month. MTCO stands for mean temperature of the coldest month. PANN stands for mean annual precipitation. P_{winter} indicates winter precipitation. OD stands for Oldest Dryas. B/A stands for Bølling–Allerød. YD stands for Younger Dryas. EH stands for early Holocene.

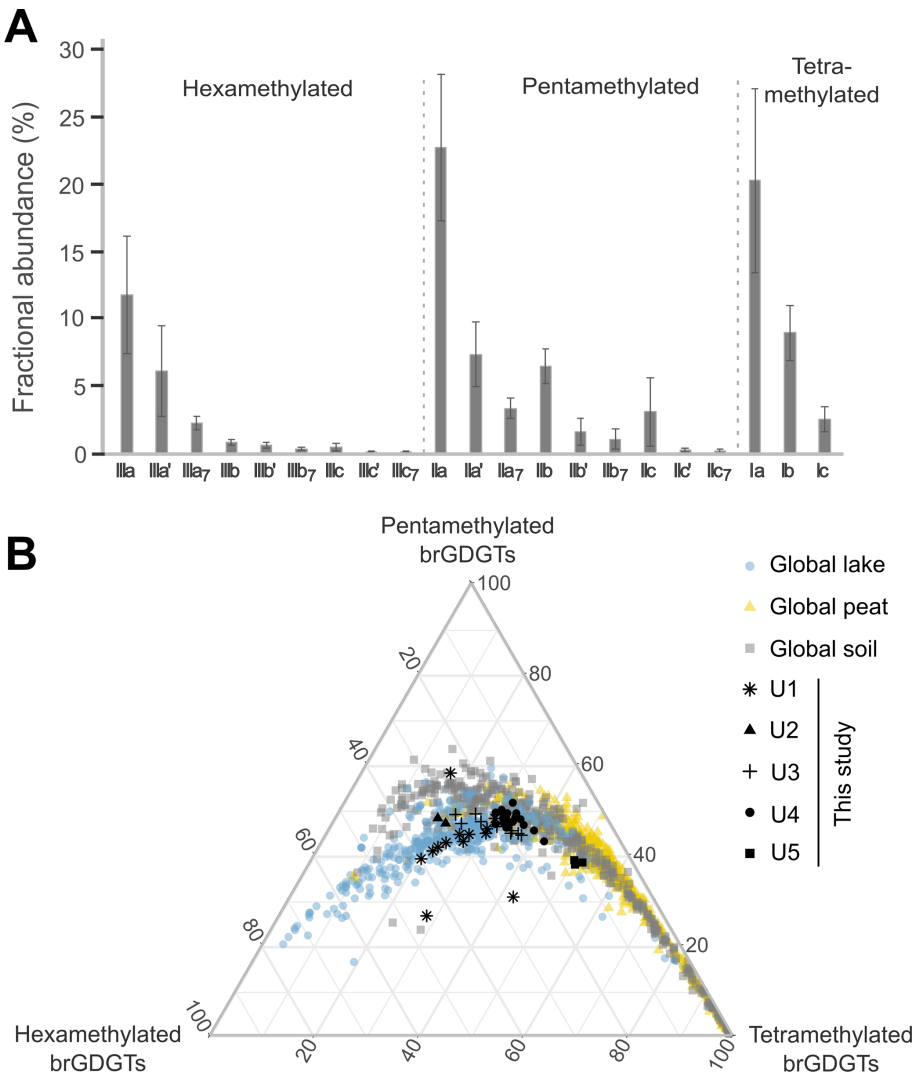

Figure 6. **(a)** Fractional abundances of tetra-, penta- and hexa-methylated brGDGTs for the Matese core. **(b)** Ternary diagram showing the fractional abundances of the tetra-, penta- and hexa-methylated brGDGTs for the Matese core (black points) and global lakes (blue points; Martínez-Sosa et al., 2021), peats (yellow circles; Naafs et al., 2017a) and soils (gray circles; Yang et al., 2014; Naafs et al., 2017b).

ues between 502–490 and 466–352 cm and is dominant at 518 and 352–338 cm (phase 4).

The degree of methylation (MBT, MBT'_{5Me}) and the cyclization ratio (CBT) also show variation along the Matese core (Fig. 7). The MBT and the MBT'_{5Me} show similar trends but different absolute values; they vary between 0.17 and 0.52 and between 0.20 and 0.63, respectively. The degree of methylation remains relatively stable, except during two phases of decrease between 534–522 and 486–458 cm and two phases with higher values at 518 cm depth and during phase 4. The CBT varies between 0.27 and 0.74. Phase 1 (535–530 cm) is characterized by high values of CBT followed by a decline until reaching a minimum between 494 and 482 cm. Following this, the CBT slightly increases; at 382 cm a slow decline is recorded and a strong increase marks phase 4.

4.4.3 Temperature reconstructions based on brGDGTs

The brGDGT-inferred reconstructed MAATs using global (Sun et al., 2011) and East African (Russell et al., 2018) lacustrine calibrations show similar trends to the MAF reconstructed using a Bayesian statistical model (Martínez-Sosa et al., 2021) and global (Raberg et al., 2021) lacustrine calibrations (Fig. 8). The values are higher than modern values, especially the values for the MAF_{Full} (Raberg et al., 2021). During phase 1 (535–530 cm; 14 600–14 500 cal BP), all calibrations show cold temperatures. Phase 2 (530–436 cm; 14 500–12 800 cal BP) is marked by an abrupt temperature increase, a stabilization for MAF_{Meth} or a decline for MAF_{Full}. Between 13 700 and 13 200 cal BP, lower temperatures are recorded with all calibrations, and from 13 100 cal BP temperatures slowly decrease until

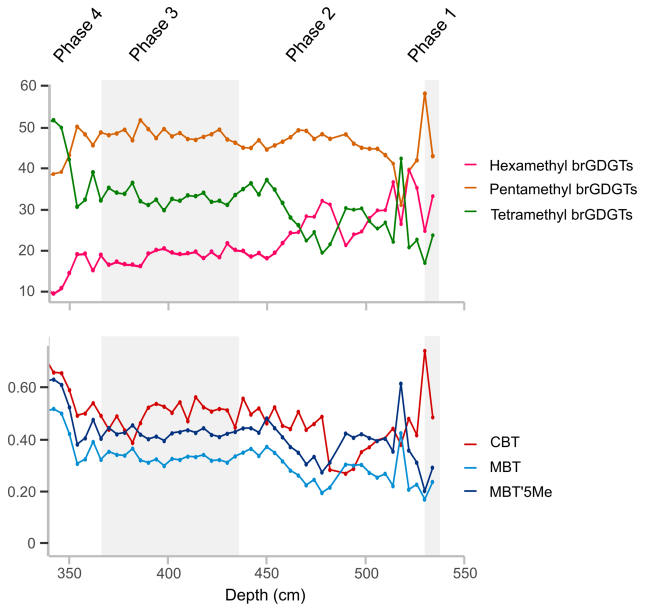

Figure 7. Fractional abundances of tetra-, penta- and hexamethylated brGDGT degree of methylation (MBT, MBT'_{5Me}) and cyclization ratio (CBT) against depth for the Matese core.

11 300 cal BP, although a slight increase is recorded between 11 900 and 11 500 cal BP. Phase 4 (367–338 cm; 11 570–11 000 cal BP) is characterized by a significant increase in temperature.

5 Discussion

5.1 Validation of age–depth model

The compilation of ages derived from the Italian pollen stratigraphy into the Matese age model is based on the main vegetation changes identified in the area during the Late Glacial. In summary, the OD in Italian pollen records (and in the present study, Fig. 4) is characterized by an open vegetation dominated by Poaceae, *Artemisia*, with a few arboreal pollen such as *Pinus* and *Juniperus* appearing (Allen et al., 2002; Vescovi et al., 2010; Drescher-Schneider et al., 2007; De Beaulieu et al., 2017; Sadori, 2018). During the B/A, a significant increase in arboreal pollen taxa, including deciduous *Quercus*, is recorded, and in the majority of records *Betula* appears (Allen et al., 2002; Drescher-Schneider et al., 2007; Vescovi et al., 2010; Sadori, 2018; this study). During the YD, an increase in Poaceae and *Artemisia* (Allen et al., 2002; Mercuri et al., 2002; Drescher-Schneider et al., 2007; Vescovi et al., 2010) and an overall decrease in arboreal pollen taxa, except in southern Italy (Allen et al., 2002; De Beaulieu et al., 2017; this study), are documented.

The ages of tephra samples and ages constrained from the pollen stratigraphy are in good agreement, contrasting results from the ^{14}C dates which are randomly scattered and systematically too young (Fig. 2). The sediments of the Matese core are mainly composed of clay with only a few plant fibers. Considering the recurrence of radiocarbon dates between 7570 and 7850 cal BP in the core interval between 420 and 360 cm depth (see Table 1), it is hypothesized that the dated organic matter may have partly originated from penetrating rootlets of plants growing during sedimentary Unit 5's deposition (Fig. 4). Indeed, aquatic plants of sedimentary Unit 5, identified with pollen, evidence a shallow water body and the development of tree species that typically grow in wetland.

Therefore, the overall age–depth model of the Matese core is based on imported, well-accepted tephra ages and one ^{14}C date of a bulk sediment sample from the bottom of the core at 534 cm (Fig. 2).

5.2 Influence of proxies and methods on climate reconstructions

5.2.1 Lake Matese climate signal reliability

Climate reconstructions are based both on pollen and brGDGTs, and some temperature discrepancies (absolute values or amplitudes) are depicted depending on the proxies (Fig. 9). The temperature amplitudes and absolute values are higher for brGDGTs (5–20 °C) than the pollen (4–10 °C) reconstructions. Pollen-inferred temperature values depend heavily on the quality of the modern pollen dataset, including the number of samples, the diversity of samples in terms of biomes and the similarity with the fossil samples (Chevalier et al., 2020). In our study, the modern database includes several modern samples from the Matese massif, and 95 samples from Italy were added to complete the dataset. Moreover, the spatial autocorrelation is low for MAT (Moran's $I < 0.34$, p value < 0.01), and climate trends are consistent between methods. Reconstructed values for temperatures are close to modern values during the warmest periods; however, precipitation is largely underestimated by all methods for the recent time period (Fig. 5). The same observation was made in Calabria in southern Italy (Trifoglietti; Joannin et al., 2012), a region also characterized by precipitation above 1700 mm. The underestimation of precipitation is certainly linked to the lack of modern samples located in very wet Mediterranean areas. Considering the brGDGT climate signal, the reconstructed temperatures are overestimated in comparison with modern values (Fig. 8). For shallow temperate lakes (< 20 m) like Lake Matese, our brGDGT reconstructions suggest values that are anomalously higher than the expected temperature due to thermal variability (seasonal and diurnal; Martínez-Sosa et al., 2021). Lake Matese is located at an altitude of 1012 m a.s.l., and the strong seasonal variability may have influenced the brGDGT distribution. Moreover, the Lake Matese climate reconstructions are based on several global lacustrine calibration datasets, which may not be well adapted to reconstruct paleotemperatures in the Mediterranean region. According to Dugerdil et al. (2021a), local calibrations perform better to reconstruct more reliable

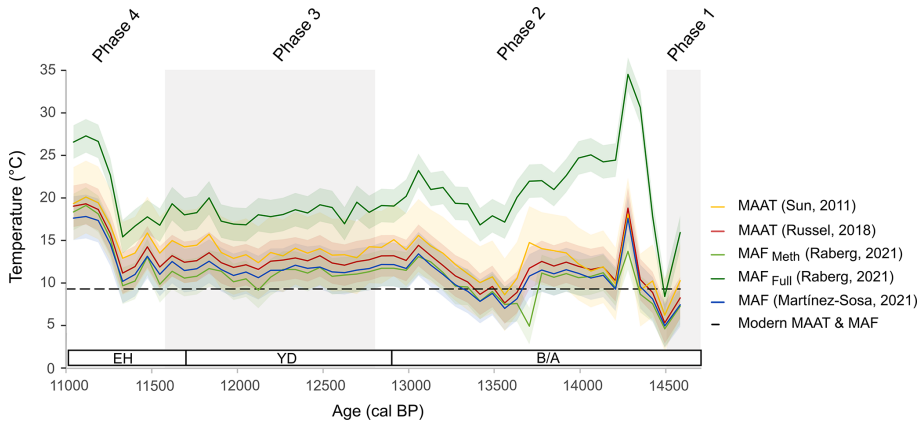

Figure 8. Mean annual air temperature (MAAT) based on global (Sun et al., 2011) and East African (Russell et al., 2018) lacustrine calibrations and mean temperature of months above freezing (MAF) based on Bayesian statistics (Martínez-Sosa et al., 2021) and global (Raberg et al., 2021) lacustrine calibrations against age for the Matese core. Shaded areas correspond to the error associated with calibrations and dashed lines correspond to modern climate values of Lake Matese. B/A stands for Bølling–Allerød. YD stands for Younger Dryas. EH stands for early Holocene.

absolute values. Unfortunately, at time of writing only a few global lacustrine calibrations are available, and a local calibration dataset for the Mediterranean region is still missing.

5.2.2 Regional climate signal reliability depending on the proxy

Climate reconstructions inferred from Lake Matese are compared to key terrestrial and marine temperature and precipitation records (Figs. 9 and 10) in a latitudinal transect in the central Mediterranean. These reconstructions for the Mediterranean region are based on different proxies. Most of those are indicators of annual temperatures, but some of them are indicators of seasonal temperature changes. For example, transfer functions based on chironomid assemblages provide estimates of mean July air temperatures (Larocque and Finsinger, 2008; Heiri et al., 2014; Samartin et al., 2017), while ostracod assemblages allow quantitative reconstruction of both January and July paleotemperatures (Marchegiano et al., 2020). Planktonic foraminifera provide estimates of spring and autumn sea surface temperatures (SSTs) (Sicre et al., 2013). Depending on the production and deposition settings, molecular biomarkers are considered indicators of annual or seasonal temperatures like brGDGTs or alkenones (Sbaffi et al., 2004; Sicre et al., 2013; Zhang et al., 2013; Max et al., 2020; Martínez-Sosa et al., 2021; this study). For precipitation (Fig. 10), fewer reconstructions are available, and they are mainly based on records of pollen (Combourieu-Nebout et al., 2013), δ^{18}O *G. bulloides* in marine sediments (Sicre et al., 2013) and δ^{18}O in speleothems (Regattieri et al., 2014). Pollen enable the reconstruction of both annual and seasonal temperatures and precipitation (e.g., Allen et al., 2002; Tarroso et al., 2016).

The comparison between climate reconstructions inferred from different proxies allows us to identify reliable regional climate signals and to reduce the bias linked to each proxy. Indeed, differences may appear for the timing or amplitudes of changes according to the type of proxy. These differences may be amplified by the proxy provenance, either marine or continental. In Fig. 9, the temperature reconstructions above 42° N are mainly based on chironomids, and the climate signal reconstructed is consistent between the sites. In southern Italy at Monticchio, climate reconstructions are based on three pollen records from the same site, and the differences in terms of amplitude and trend are clearly evidenced (Fig. 9i). These differences are linked to the differences in the core location in the lake and the pollen sample resolution (Allen et al., 2002). The closer the core is to the center of the lake (dark blue, Fig. 9i), the better the regional vegetation record and therewith a possible regional climate signal (Peyron et al., 2005). Between 41 and 36° N, SSTs were reconstructed from foraminifera and/or alkenones analyzed from marine cores (Sbaffi et al., 2004; Sicre et al., 2013). Alkenone-based SSTs show a low amplitude of 2–3 °C between the B/A and the YD periods, whereas foraminifera-based reconstructions of seasonal temperature show differences of 5–10 °C between the B/A and the YD. The differences are linked to their respective methods. For alkenones, the estimation of SSTs are based on the molecular biomarker of the C_{37} alkenone unsaturation ($U^{K'}_{37}$), whereas for foraminifera they are calculated with the MAT method and depend on the occurrence of modern analogues (Sicre et al., 2013).

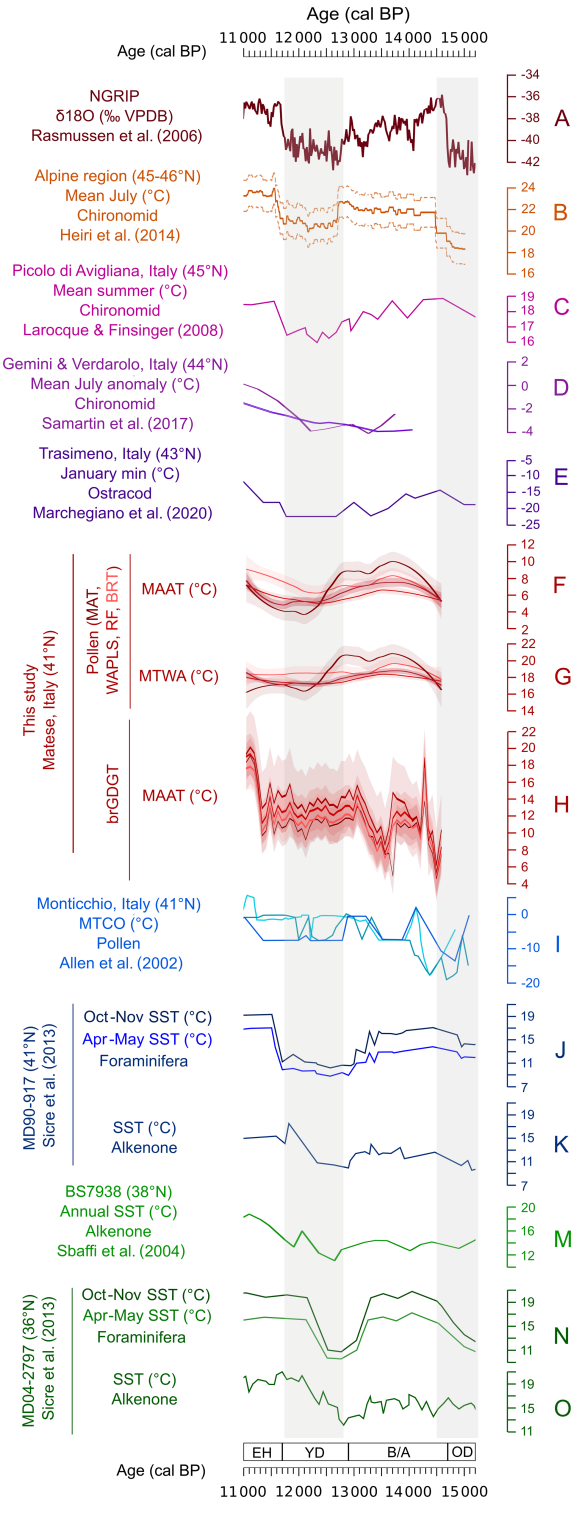

Figure 9. Synthesis of temperature records inferred from different proxies in Italy from 15 000 to 11 000 cal BP and comparison with the NGRIP ice core record. MAAT stands for mean annual air temperature. MTWA stands for mean temperature of the warmest month. MTCO stands for mean temperature of the coldest month. OD stands for Oldest Dryas. B/A stands for Bølling–Allerød. YD stands for Younger Dryas. EH stands for early Holocene.

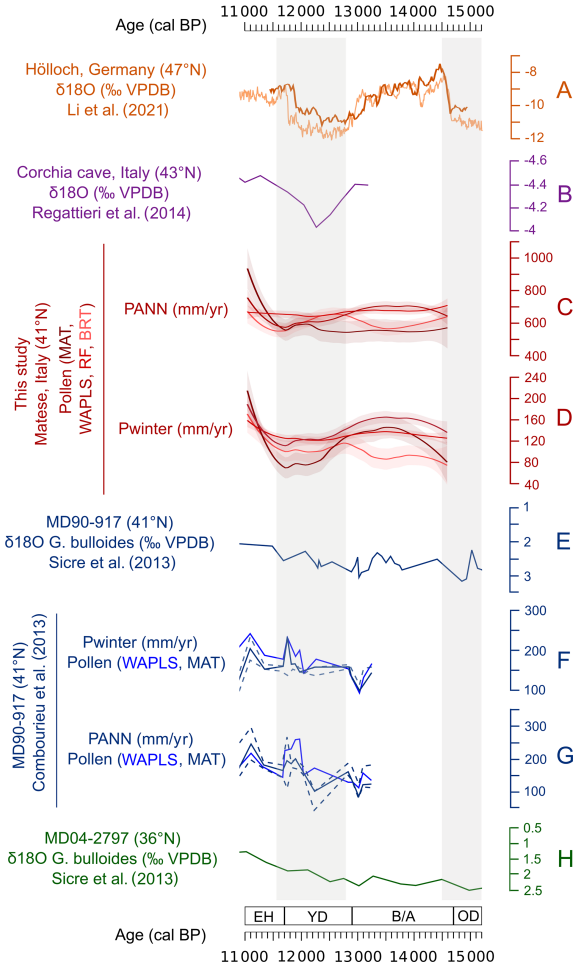

Figure 10. Synthesis of precipitation records inferred from different proxies in Italy from 15 000 to 11 000 cal BP. PANN stands for mean annual precipitation. P_{winter} is winter precipitation. OD stands for Oldest Dryas. B/A stands for Bølling–Allerød. YD stands for Younger Dryas. EH stands for early Holocene.

5.3 Climate changes during the Late Glacial in Italy

5.3.1 Bølling–Allerød warming

The age of transition between the OD and the Bølling–Allerød interstadial is estimated at around 14 700 cal BP based on the NGRIP ice core chronology (Rasmussen et al., 2014). In Italy, an abrupt warming is evidenced at ca. 14 700 cal BP (Fig. 9). The differences between the different reconstructions seem related to the type of proxy used rather than latitude. The transition is not obvious in the temperature reconstructions based on alkenones (Fig. 9m and o; Sbaffi et al., 2004; Sicre et al., 2013), whereas it is well marked in reconstructions based on foraminifera (Fig. 9n; Sicre et al., 2013) and pollen assemblages (Desprat et al., 2013) from the same cores. According to Sicre et al. (2013), alkenone-inferred SSTs could be biased during the early deglaciation due to water stratification inducing warming of

the thin surface water layers where small-sized nanophytoplankton grow. Except for temperature reconstructions based on alkenones, all the records show an increase in the temperature at the OD–B/A transition (Larocque and Finsinger, 2008; Sicre et al., 2013; Heiri et al., 2014; Marchegiano et al., 2020). The transition, although marked, seems more progressive in the Italian records than in Greenland ice core, but the low resolution of some records can favor this trend. In terms of precipitation (Fig. 10), few records are available in Italy, but no significant changes are recorded around 14 700 cal BP by δ^{18}O *G. bulloides* (Sicre et al., 2013) and pollen transfer functions (Desprat et al., 2013; this study).

The Bølling–Allerød interstadial is a warm interstadial period interrupted by several cold-climate oscillations (Rasmussen et al., 2014). According to the synthesis by Moreno et al. (2014), the Bølling was cooler than the Allerød in the southern Mediterranean compared to the warmer northern Mediterranean. In Italy, above 42° N, temperature trends are complex to interpret: some records show an increase in temperature (Fig. 9b; Heiri et al., 2014), whereas other records show a decline (Fig. 9c and e; Larocque and Finsinger, 2008; Marchegiano et al., 2020). At Matese, pollen- and brGDGT-inferred temperatures decrease (Fig. 9f–h), whereas in the southern part of Italy, there are no significant changes during the B/A (Fig. 9i–o; Allen et al., 2002; Sbaffi et al., 2004; Sicre et al., 2013). Temperature reconstructions in Italy show no distinct difference between the Bølling and the Allerød with respect to latitude. In terms of amplitude, several studies (Renssen and Isarin, 2001; Heiri et al., 2014; Moreno et al., 2014) suggest that there were fewer contrasts in temperatures during the B/A in southern Europe in comparison with northern Europe. Once again, this difference is not clear in Italy (Fig. 9). At Matese, a significant decrease in brGDGT-inferred temperature is recorded at 13 700–13 200 cal BP (Fig. 9h). This change could be attributed to a colder period such as the Older Dryas or the inter-Allerød cold period, two short periods characterized by colder conditions in the Greenland ice core records at 14 000 and 13 100 cal BP, respectively (Rasmussen et al., 2014). However, this cooling event does not appear at the same time in the Matese climate curve based on pollen, and it is only vaguely recorded in other Italian records (Fig. 9). We suggest that this change could be attributed to changes in local conditions that are visible in a lithology change (sedimentary Unit 2, Fig. 4). Indeed, brGDGT distribution and origin can differ according to the type of wetland, water level or vegetation changes (Martínez-Sosa et al., 2021; Robles et al., 2022). In terms of precipitation (Fig. 10), no significant changes occur during the B/A in Italy, as suggested previously by Renssen and Isarin (2001) for southern Europe. The Alpine region seems instead to record wetter conditions during the B/A (Barton et al., 2018; Li et al., 2021).

5.3.2 A marked Younger Dryas cold event throughout Italy

The onset of the YD is estimated around 12 900 cal BP according to the Greenland ice core chronology (Rasmussen et al., 2014). In Italy, above 42° N, the transition between the B/A and the YD is progressive in terms of temperatures except for chironomid records (Fig. 9b; Heiri et al., 2014). At Matese, pollen-based reconstructions show a progressive decline in temperatures with all methods except the MAT (Fig. 9f and g). For this method, the transition is more abrupt, but this difference can be attributed to the application of the biome constraint. BrGDGT-based reconstructions record a steady decrease during the YD or no significant changes according to the calibrations used (Fig. 9h). For southern Italian records, the transition is more abrupt and particularly marked in the foraminifera record in contrast to alkenone-based reconstructions (Fig. 9j–o; Sbaffi et al., 2004; Sicre et al., 2013). In terms of precipitation (Fig. 10), the northern Italian speleothem records show an abrupt transition (Regattieri et al., 2014; Li et al., 2021), whereas the southern Italian pollen and isotope records do not reveal significant changes (Sicre et al., 2013; Combourieu-Nebout et al., 2013; Desprat et al., 2013).

The YD is characterized by cold conditions in the Northern Hemisphere from 12 900 to 11 700 cal BP (Rasmussen et al., 2014). As previously mentioned for the B/A, several studies (Renssen and Isarin, 2001; Heiri et al., 2014; Moreno et al., 2014) suggest that temperatures during the YD are less contrasted in the south of Europe in comparison with the north. In Italy as a whole (Fig. 9), a decline in temperatures is recorded in all records.

At Matese, a decrease in temperatures is evidenced by the pollen-based reconstructions, but it is less clear from the brGDGT-based reconstructions. The difference of climate signals may be related to different sources between both proxies. Pollen record local, extra-local and regional vegetation (Jacobson and Bradshaw, 1981). The basin size of the Lake Matese is larger than 5 ha, which suggests a signal of regional vegetation rather than local (Jacobson and Bradshaw, 1981). Moreover, the YD is marked by a large proportion of herbaceous taxa (Fig. 4) and favors the catching of regional pollen (Jacobson and Bradshaw, 1981). By contrast, brGDGTs are produced in the lake or in the catchment area (Russell et al., 2018; Martin et al., 2019) and thus are local contributors. Moreover, the YD is characterized by high erosion rates in the catchment (Fig. 4), which could favor greater soil-derived brGDGTs and induce a warm bias in temperatures (Martínez-Sosa et al., 2021). Indeed, the distributions of brGDGTs differ according to sample type and could differ between lake sediments and catchment soils (Loomis et al., 2011, 2014; Buckles et al., 2014; Russell et al., 2018; Martin et al., 2019; Martínez-Sosa et al., 2021; Raberg et al., 2022). Soil sediments generally exhibit less hexa-methylated brGDGTs and more tetra-methylated

brGDGTs than lake sediments (Loomis et al., 2011, 2014; Buckles et al., 2014; Russell et al., 2018; Martin et al., 2019; Martínez-Sosa et al., 2021). However, an increase in tetra-methylated brGDGTs is mainly associated with an increase in temperatures in soils and lake sediments (Russell et al., 2018). At Matese, the YD is characterized by a decrease in hexa-methylated brGDGTs and a slight increase in tetra-methylated brGDGTs. These differences may have affected the annual temperature reconstructions by inducing a warm bias in temperatures during the YD. Furthermore, soil-derived brGDGTs may also be affected by changes in pH, moisture, soil compounds and vegetation in the catchment of Lake Matese (Davtian et al., 2016; Martin et al., 2019; Liang et al., 2019; Dugerdil et al., 2021a). Soil samples without vegetation cover are also more sensitive to seasonal changes than soil samples with grass and forest cover (Liang et al., 2019). Therefore, soils with vegetation cover allow a better reconstruction of global temperatures (Liang et al., 2019). Since at Matese the YD is characterized by open vegetation, soil-derived brGDGTs could also have been affected by seasonal temperature changes due to a sparse vegetation, and this effect is superimposed onto changes in the sources of brGDGTs in lake sediments.

Contrasted patterns are also recorded at Monticchio (Fig. 9i) by the three different climate variables used for pollen-based temperature reconstructions: a decrease in winter temperature is reconstructed for two lake cores, while a fen core external to the lake, which should record the local vegetation signal, does not reveal the temperature decline during the YD (Allen et al., 2002). However, the two other cores clearly show a temperature decrease, which is why we consider a winter temperature decrease during the YD at Monticchio. In southern Italian records, temperature reconstructions based on alkenones, foraminifera and pollen (Sbaffi et al., 2004; Desprat et al., 2013; Sicre et al., 2013) show a shorter YD than in the north. For alkenone-based reconstructions, an increase in temperatures is even recorded at the end of the YD. In continental records of southern Italy (Allen et al., 2002), this trend is only recorded at Monticchio (one core only) and does not appear at Matese. Nonetheless, this hypothesis is only based on marine records and should be investigated through continental records in southern Italy.

In terms of precipitation, the marine sequences located south of 42° N record a slight increase for proxies based on pollen (Fig. 9g and h; Combourieu-Nebout et al., 2013) and on δ^{18}O *G. bulloides* data (Fig. 9f and i; Sicre et al., 2013) during the YD. However, no significant change occurs at Matese for PANN (Fig. 10c), and on the contrary a low decline is recorded for P_{winter} towards the end of the YD (Fig. 10d). Above 42° N, a precipitation decrease during the YD is recorded by two sites at the Hölloch and Corchia caves (Fig. 10a and b; Regattieri et al., 2014; Li et al., 2021). According to the model outputs of Rea et al. (2020), drier conditions occurred in northern Europe, whereas wetter conditions prevailed in southern Europe, mainly during winter and in the south of Italy, the Dinaric Alps and northern Turkey. This pattern is consistent with our reconstruction, but the limit between the northern and the southern regions is closer to 42° N.

The transition between the YD and the Holocene is recorded around 11 700 cal BP by Greenland ice core records (Rasmussen et al., 2014). In Italy, an important increase in temperature is recorded in all records (Fig. 9) that appears earlier (700–400 years) in southern sites (Sbaffi et al., 2004; Sicre et al., 2013). In terms of precipitation, marine records south of 42° N continue to record a slight increase in precipitation (Fig. 10e–h; Combourieu-Nebout et al., 2013; Sicre et al., 2013), and in northern sites an increase in precipitation is recorded (Fig. 10a–d; Regattieri et al., 2014; Li et al., 2021; this study).

5.4 Atmospheric processes during the Late Glacial in the central Mediterranean

According to several studies, climate changes during the Late Glacial show differences in temperatures between southern and central Europe (Renssen and Isarin, 2001; Heiri et al., 2014; Moreno et al., 2014). In Italy (Fig. 9), climate reconstructions do not show latitudinal differences in terms of temperature. The B/A is marked by warm conditions and the YD by cold conditions even in southern Italy. Climate reconstructions for eastern and central southern Europe from Heiri et al. (2014) are not consistent with our results; this is probably because, while two of their chironomid records are located in northern Italy and one in Bulgaria, none consider southern Italy. In the study of Moreno et al. (2014), only the record of Monticchio is used for the south of Italy during the Late Glacial, which may explain the differences in our study. Considering precipitation, several studies suggest no significant changes during the B/A but drier conditions in northern Europe and wetter conditions in southern Europe during the YD. In Italy (Fig. 10), we observe the same dynamics during the B/A and the YD.

Several studies (Renssen and Isarin, 2001; Moreno et al., 2014; Rea et al., 2020) explain that during cold periods of the Late Glacial (OD, YD) the polar frontal jet stream moved southward with a weak Atlantic meridional overturning circulation (AMOC) (Rea et al., 2020; Renssen and Isarin, 2001; Moreno et al., 2014). The incursion of cold air masses is recorded until the south of Italy; however, during the YD, dry conditions are not reconstructed for this region. According to Rea et al. (2020), a relocation of Atlantic storm tracks in the Mediterranean is induced by the Fennoscandian ice sheet and the North European Plain, which created a topographic barrier and a high-pressure region during the YD. The presence of Atlantic storm tracks into the Mediterranean could have favored wetter conditions in the South of Italy during the YD. Our study suggests a limit around 42° N, with drier conditions in northern Italy and slightly wetter conditions in southern Italy during the YD. A latitude limit

at 40° N was previously discussed by Magny et al. (2013) for the Holocene. These echoing limits over time in Italy inevitably reinforce Italy's key position to archive proxies catching atmospheric patterns.

By contrast, during the B/A the North Atlantic sea ice has a more northerly position, inducing a northward shift of the polar frontal jet stream (Renssen and Isarin, 2001). The incursion of warm air masses is recorded in all of Italy; however, no significant changes in annual precipitation occur. Our study does not suggest the location of Atlantic storm tracks in Italy during the B/A, although at Matese winter precipitation was higher in most pollen-based climate reconstructions. However, very few records and climatic models reconstructing precipitation are available in Europe and the Mediterranean region for this period. Further investigations are necessary to fully understand the atmospheric processes and precipitation dynamic in Europe, mainly during the B/A.

6 Conclusions

This study provides a quantitative climate reconstruction for the Late Glacial period in central southern Europe, inferred from a multi-proxy and multi-method approach based on the Lake Matese record. The comparison of the Lake Matese climate reconstructions based on brGDGTs and pollen and their comparison with regional terrestrial and marine climate reconstructions allow us to draw the following conclusions.

- For the first time, pollen and brGDGTs were combined to reconstruct climate changes in the Mediterranean region during the Late Glacial. Temperature trends reconstructed with these proxies are consistent except during the YD. Both proxies show a marked cold OD, an increase in temperatures during the B/A, and an abrupt transition to warmer conditions for the Holocene. During the YD, pollen-based reconstructions show a decrease in temperatures, whereas brGDGT-based reconstructions show no significant changes.

- Comparison with regional climate records of Italy reveals that there are no latitudinal differences during the B/A and the YD in terms of temperatures. The B/A is marked by an increase in temperature and the YD is characterized by cold conditions in all Italy. By contrast, precipitation does not show changes during the B/A, and a slight increase in precipitation during the YD is recorded in southern Italy below latitude 42° N.

- Cold conditions during the YD in Italy may be linked to the southward position of North Atlantic sea-ice and of the polar frontal jet stream. The low increase in precipitation during the YD may be linked to relocation of Atlantic storm tracks into the Mediterranean, induced by the Fennoscandian ice sheet and the North European Plain. We identified the latitude 42° N as a limit between dry conditions in northern Italy and slightly wetter conditions in southern Italy during the YD. By contrast, warm conditions during the B/A may be linked to the northward position of North Atlantic sea-ice and of the polar frontal jet stream.

In summary, this study allowed us to document and discuss past climate changes in Italy while contributing to the debate about the atmospheric processes in southern Europe. The latitude and of 40–42° N appears as a key junction point between wetter conditions in southern Italy and drier conditions in northern Italy during the YD and during the early to mid Holocene (Magny et al., 2013). However, further robust paleoclimate studies are needed to provide (1) high-resolution reconstructions based on several proxies in northern Italy, (2) new records for central Italy (between 41 and 43° N), (3) new continental records for southern Italy (below 41° N), and (4) more model outputs at regional scales with transient simulations, if possible, mainly during the B/A and the YD.

Data availability. GDGT data produced and analyzed in this study are available in Table S2, and the pollen data will be available on EPD, Neotoma and PANGAEA. Tephra glass data are available in Table S3.

Supplement. The supplement related to this article is available online at: https://doi.org/10.5194/cp-19-493-2023-supplement.

Author contributions. MR contributed to the conceptualization, field work, laboratory work, formal analysis, writing of the draft manuscript, review and funding acquisition. SJ, OP and EB contributed to the conceptualization, field work, supervision, review and funding acquisition. GM contributed to the conceptualization, supervision, review and funding acquisition. SW contributed to the laboratory work, formal analysis, review and funding acquisition. OA and MB did laboratory work. BV contributed to the supervision of laboratory work and review. BP contributed to the field work. SAA contributed to the coordination of laboratory work. LC and SG contributed to the conceptualization and review. JLdB, LD and AC contributed to the review.

Competing interests. The contact author has declared that none of the authors has any competing interests.

Disclaimer. Publisher's note: Copernicus Publications remains neutral with regard to jurisdictional claims in published maps and institutional affiliations.

Acknowledgements. The authors would like to thank Julien Didier for providing magnetic susceptibility measurements and Laurent Bouby and Isabelle Figueral for providing seed and wood iden-

tification data used for radiocarbon dating. The authors would like to express their appreciation to Gwenaël Magne, Thierry Pastor and Benoît Brossier for logistical support during fieldwork and Anne-Lise Develle and Claire Blanchet for help during XRF analysis. We would like to thank Sandrine Canal and Sylvie Rouland for support during pollen sample preparation. This is ISEM contribution no. 2022-266.

Financial support. This research was co-founded by the International PhD course "Agriculture Technologies and Biotechnologies" (34° Cycle, Code: DOT1339335). Financial support for this study was provided by EFFICACE project from EC2CO INSU CNRS (PI: Odile Peyron) and ERJ ClimMatese from LabEx CeMEB (PI: Mary Robles). Travel between Italy and France was financed by VINCI funding of the Università Italo Francese (UIF). Conference funding was provided by the Association des Palynologues de Langue Française (APLF).

Review statement. This paper was edited by Nathalie Combourieu Nebout and reviewed by Jens Holtvoeth and one anonymous referee.

References

Allen, J. R. M., Watts, W. A., McGee, E., and Huntley, B.: Holocene environmental variability-the record from Lago Grande di Monticchio, Italy, Quatern. Int., 88, 69–80, 2002.

Ammann, B., Birks, H. J. B., Brooks, S. J., Eicher, U., von Grafenstein, U., Hofmann, W., Lemdahl, G., Schwander, J., Tobolski, K., and Wick, L.: Quantification of biotic responses to rapid climatic changes around the Younger Dryas – a synthesis, Palaeogeogr. Palaeocl., 159, 313–347, https://doi.org/10.1016/S0031-0182(00)00092-4, 2000.

Aucelli, P. P. C., Cesarano, M., Di Paola, G., Filocamo, F., and Rosskopf, C. M.: Geomorphological map of the central sector of the Matese Mountains (Southern Italy): an example of complex landscape evolution in a Mediterranean mountain environment, J. Maps, 9, 604–616, https://doi.org/10.1080/17445647.2013.840054, 2013.

Barton, C. M., Aura Tortosa, J. E., Garcia-Puchol, O., Riel-Salvatore, J. G., Gauthier, N., Vadillo Conesa, M., and Pothier Bouchard, G.: Risk and resilience in the late glacial: A case study from the western Mediterranean, Quaternary Sci. Rev., 184, 68–84, https://doi.org/10.1016/j.quascirev.2017.09.015, 2018.

Beug, H.-J.: Leitfaden der Pollenbestimmung für Mitteleuropa und angrenzende Gebiete, Friedrich Pfeil, München, 542 pp., ISBN 10 3899370430, 13 978-3899370430, 2004.

Blaauw, M.: Methods and code for 'classical' age-modelling of radiocarbon sequences, Quatern. Geochronol., 5, 512–518, https://doi.org/10.1016/j.quageo.2010.01.002, 2010.

Blaga, C. I., Reichart, G.-J., Lotter, A. F., Anselmetti, F. S., and Sinninghe Damsté, J. S.: A TEX 86 lake record suggests simultaneous shifts in temperature in Central Europe and Greenland during the last deglaciation: A Swiss TEX 86 Lake Record, Geophys. Res. Lett., 40, 948–953, https://doi.org/10.1002/grl.50181, 2013.

Breiman, L.: Random Forests, Mach. Learn., 45, 5–32, https://doi.org/10.1023/A:1010933404324, 2001.

Bronk Ramsey, C., Albert, P. G., Blockley, S. P. E., Hardiman, M., Housley, R. A., Lane, C. S., Lee, S., Matthews, I. P., Smith, V. C., and Lowe, J. J.: Improved age estimates for key Late Quaternary European tephra horizons in the RESET lattice, Quaternary Sci. Rev., 118, 18–32, https://doi.org/10.1016/j.quascirev.2014.11.007, 2015.

Buckles, L. K., Weijers, J. W. H., Verschuren, D., and Sinninghe Damsté, J. S.: Sources of core and intact branched tetraether membrane lipids in the lacustrine environment: Anatomy of Lake Challa and its catchment, equatorial East Africa, Geochim. Cosmochim. Ac., 140, 106–126, https://doi.org/10.1016/j.gca.2014.04.042, 2014.

Carranza, M. L., Frate, L., and Paura, B.: Structure, ecology and plant richness patterns in fragmented beech forests, Plant Ecol. Divers., 5, 541–551, https://doi.org/10.1080/17550874.2012.740509, 2012.

Castañeda, I. S. and Schouten, S.: A review of molecular organic proxies for examining modern and ancient lacustrine environments, Quaternary Sci. Rev., 30, 2851–2891, https://doi.org/10.1016/j.quascirev.2011.07.009, 2011.

Chevalier, M., Davis, B. A. S., Heiri, O., Seppä, H., Chase, B. M., Gajewski, K., Lacourse, T., Telford, R. J., Finsinger, W., Guiot, J., Kühl, N., Maezumi, S. Y., Tipton, J. R., Carter, V. A., Brussel, T., Phelps, L. N., Dawson, A., Zanon, M., Vallé, F., Nolan, C., Mauri, A., de Vernal, A., Izumi, K., Holmström, L., Marsicek, J., Goring, S., Sommer, P. S., Chaput, M., and Kupriyanov, D.: Pollen-based climate reconstruction techniques for late Quaternary studies, Earth-Sci. Rev., 210, 103384, https://doi.org/10.1016/j.earscirev.2020.103384, 2020.

Combourieu-Nebout, N., Peyron, O., Bout-Roumazeilles, V., Goring, S., Dormoy, I., Joannin, S., Sadori, L., Siani, G., and Magny, M.: Holocene vegetation and climate changes in the central Mediterranean inferred from a high-resolution marine pollen record (Adriatic Sea), Clim. Past, 9, 2023–2042, https://doi.org/10.5194/cp-9-2023-2013, 2013.

Coope, G. R. and Lemdahl, G.: Regional differences in the Lateglacial climate of northern Europe based on coleopteran analysis, J. Quaternary Sci., 10, 391–395, https://doi.org/10.1002/jqs.3390100409, 1995.

Davtian, N., Ménot, G., Bard, E., Poulenard, J., and Podwojewski, P.: Consideration of soil types for the calibration of molecular proxies for soil pH and temperature using global soil datasets and Vietnamese soil profiles, Org. Geochem., 101, 140–153, https://doi.org/10.1016/j.orggeochem.2016.09.002, 2016.

Davtian, N., Bard, E., Ménot, G., and Fagault, Y.: The importance of mass accuracy in selected ion monitoring analysis of branched and isoprenoid tetraethers, Org. Geochem., 118, 58–62, https://doi.org/10.1016/j.orggeochem.2018.01.007, 2018.

Dearing Crampton-Flood, E., Tierney, J. E., Peterse, F., Kirkels, F. M. S. A., and Sinninghe Damsté, J. S.: BayMBT: A Bayesian calibration model for branched glycerol dialkyl glycerol tetraethers in soils and peats, Geochim. Cosmochim. Ac., 268, 142–159, https://doi.org/10.1016/j.gca.2019.09.043, 2020.

De'ath, G.: Boosted trees for ecological modeling and prediction, Ecology, 88, 243–251, https://doi.org/10.1890/0012-9658(2007)88[243:BTFEMA]2.0.CO;2, 2007.

De Beaulieu, J.-L., Brugiapaglia, E., Joannin, S., Guiter, F., Zanchetta, G., Wulf, S., Peyron, O., Bernardo, L., Didier, J., Stock, A., Rius, D., and Magny, M.: Lateglacial-Holocene abrupt vegetation changes at Lago Trifoglietti in Calabria, Southern Italy: The setting of ecosystems in a refugial zone, Quaternary Sci. Rev., 158, 44–57, https://doi.org/10.1016/j.quascirev.2016.12.013, 2017.

De Jonge, C., Hopmans, E. C., Zell, C. I., Kim, J.-H., Schouten, S., and Sinninghe Damsté, J. S.: Occurrence and abundance of 6-methyl branched glycerol dialkyl glycerol tetraethers in soils: Implications for palaeoclimate reconstruction, Geochim. Cosmochim. Ac., 141, 97–112, https://doi.org/10.1016/j.gca.2014.06.013, 2014.

Desprat, S., Combourieu-Nebout, N., Essallami, L., Sicre, M. A., Dormoy, I., Peyron, O., Siani, G., Bout Roumazeilles, V., and Turon, J. L.: Deglacial and Holocene vegetation and climatic changes in the southern Central Mediterranean from a direct land–sea correlation, Clim. Past, 9, 767–787, https://doi.org/10.5194/cp-9-767-2013, 2013.

Ding, S., Schwab, V. F., Ueberschaar, N., Roth, V.-N., Lange, M., Xu, Y., Gleixner, G., and Pohnert, G.: Identification of novel 7-methyl and cyclopentanyl branched glycerol dialkyl glycerol tetraethers in lake sediments, Org. Geochem., 102, 52–58, https://doi.org/10.1016/j.orggeochem.2016.09.009, 2016.

Drescher-Schneider, R., de Beaulieu, J.-L., Magny, M., Walter-Simonnet, A.-V., Bossuet, G., Millet, L., Brugiapaglia, E., and Drescher, A.: Vegetation history, climate and human impact over the last 15,000 years at Lago dell'Accesa (Tuscany, Central Italy), Veget. Hist. Archaeobot., 16, 279–299, https://doi.org/10.1007/s00334-006-0089-z, 2007.

Dugerdil, L., Joannin, S., Peyron, O., Jouffroy-Bapicot, I., Vannière, B., Boldgiv, B., Unkelbach, J., Behling, H., and Ménot, G.: Climate reconstructions based on GDGT and pollen surface datasets from Mongolia and Baikal area: calibrations and applicability to extremely cold–dry environments over the Late Holocene, Clim. Past, 17, 1199–1226, https://doi.org/10.5194/cp-17-1199-2021, 2021a.

Dugerdil, L., Ménot, G., Peyron, O., Jouffroy-Bapicot, I., Ansanay-Alex, S., Antheaume, I., Behling, H., Boldgiv, B., Develle, A.-L., Grossi, V., Magail, J., Makou, M., Robles, M., Unkelbach, J., Vannière, B., and Joannin, S.: Late Holocene Mongolian climate and environment reconstructions from brGDGTs, NPPs and pollen transfer functions for Lake Ayrag: Paleoclimate implications for Arid Central Asia, Quaternary Sci. Rev., 273, 107235, https://doi.org/10.1016/j.quascirev.2021.107235, 2021b.

Duprat-Oualid, F., Bégeot, C., Peyron, O., Rius, D., Millet, L., and Magny, M.: High-frequency vegetation and climatic changes during the Lateglacial inferred from the Lapsou pollen record (Cantal, southern Massif Central, France), Quatern. Int., 636, 69–80, https://doi.org/10.1016/j.quaint.2022.04.012, 2022.

Elith, J., Leathwick, J. R., and Hastie, T.: A working guide to boosted regression trees, J. Anim. Ecol., 77, 802–813, https://doi.org/10.1111/j.1365-2656.2008.01390.x, 2008.

Faegri, K., Kaland, P. E., and Krzywinski, K.: Textbook of pollen analysis, John Wiley & Sons, Chichester, ISBN 0471921785, 1989.

Ferranti, L., Milano, G., Burrato, P., Palano, M., and Cannavò, F.: The seismogenic structure of the 2013–2014 Matese seismic sequence, Southern Italy: implication for the geometry of the Apennines active extensional belt, Geophys. J. Int., 201, 823–837, https://doi.org/10.1093/gji/ggv053, 2015.

Ferrarini, F., Boncio, P., de Nardis, R., Pappone, G., Cesarano, M., Aucelli, P. P. C., and Lavecchia, G.: Segmentation pattern and structural complexities in seismogenic extensional settings: The North Matese Fault System (Central Italy), J. Struct. Geol., 95, 93–112, https://doi.org/10.1016/j.jsg.2016.11.006, 2017.

Finsinger, W., Heiri, O., Valsecchi, V., Tinner, W., and Lotter, A. F.: Modern pollen assemblages as climate indicators in southern Europe, Global Ecol. Biogeogr., 16, 567–582, https://doi.org/10.1111/j.1466-8238.2007.00313.x, 2007.

Fiorillo, F. and Doglioni, A.: The relation between karst spring discharge and rainfall by cross-correlation analysis (Campania, southern Italy), Hydrogeol. J., 18, 1881–1895, https://doi.org/10.1007/s10040-010-0666-1, 2010.

Fiorillo, F. and Pagnozzi, M.: Recharge processes of Matese karst massif (southern Italy), Environ. Earth Sci., 74, 7557–7570, https://doi.org/10.1007/s12665-015-4678-y, 2015.

Galli, P., Giaccio, B., Messina, P., Peronace, E., Amato, V., Naso, G., Nomade, S., Pereira, A., Piscitelli, S., Bellanova, J., Billi, A., Blamart, D., Galderisi, A., Giocoli, A., Stabile, T., and Thil, F.: Middle to Late Pleistocene activity of the northern Matese fault system (southern Apennines, Italy), Tectonophysics, 699, 61–81, https://doi.org/10.1016/j.tecto.2017.01.007, 2017.

Gandouin, E., Rioual, P., Pailles, C., Brooks, S. J., Ponel, P., Guiter, F., Djamali, M., Andrieu-Ponel, V., Birks, H. J. B., Leydet, M., Belkacem, D., Haas, J. N., Van der Putten, N., and de Beaulieu, J. L.: Environmental and climate reconstruction of the late-glacial-Holocene transition from a lake sediment sequence in Aubrac, French Massif Central: Chironomid and diatom evidence, Palaeogeogr. Palaeocl., 461, 292–309, https://doi.org/10.1016/j.palaeo.2016.08.039, 2016.

Guarino, R., Bazan, G., and Paura, B.: Downy-Oak Woods of Italy: Phytogeographical Remarks on a Controversial Taxonomic and Ecologic Issue, in: Warm-Temperate Deciduous Forests around the Northern Hemisphere, edited by: Box, E. O. and Fujiwara, K., Springer International Publishing, Cham, 139–151, https://doi.org/10.1007/978-3-319-01261-2_7, 2015.

Guiot, J.: Methodology of the last climatic cycle reconstruction in France from pollen data, Palaeogeogr. Palaeocl., 80, 49–69, https://doi.org/10.1016/0031-0182(90)90033-4, 1990.

Guiot, J., de Beaulieu, J. L., Cheddadi, R., David, F., Ponel, P., and Reille, M.: The climate in Western Europe during the last Glacial/Interglacial cycle derived from pollen and insect remains, Palaeogeogr. Palaeocl., 103, 73–93, https://doi.org/10.1016/0031-0182(93)90053-L, 1993.

Heiri, O., Brooks, S. J., Renssen, H., Bedford, A., Hazekamp, M., Ilyashuk, B., Jeffers, E. S., Lang, B., Kirilova, E., Kuiper, S., Millet, L., Samartin, S., Toth, M., Verbruggen, F., Watson, J. E., van Asch, N., Lammertsma, E., Amon, L., Birks, H. H., Birks, H. J. B., Mortensen, M. F., Hoek, W. Z., Magyari, E., Muñoz Sobrino, C., Seppä, H., Tinner, W., Tonkov, S., Veski, S., and Lotter, A. F.: Validation of climate model-inferred regional temperature change for late-glacial Europe, Nat. Commun., 5, 4914, https://doi.org/10.1038/ncomms5914, 2014.

Heiri, O., Ilyashuk, B., Millet, L., Samartin, S., and Lotter, A. F.: Stacking of discontinuous regional palaeoclimate records: Chironomid-based summer temperatures from the Alpine region, Holocene, 25, 137–149, https://doi.org/10.1177/0959683614556382, 2015.

Hepp, J., Wüthrich, L., Bromm, T., Bliedtner, M., Schäfer, I. K., Glaser, B., Rozanski, K., Sirocko, F., Zech, R., and Zech, M.: How dry was the Younger Dryas? Evidence from a coupled δ^2H–δ^{18}O biomarker paleohygrometer applied to the Gemündener Maar sediments, Western Eifel, Germany, Clim. Past, 15, 713–733, https://doi.org/10.5194/cp-15-713-2019, 2019.

Hijmans, R. J., Phillips, S., Leathwick, J., and Elith, J.: dismo: Species Distribution Modeling, https://rspatial.org/raster/sdm/ (last access: 13 December 2022), 2021.

Hopmans, E. C., Schouten, S., and Sinninghe Damsté, J. S.: The effect of improved chromatography on GDGT-based palaeoproxies, Org. Geochem., 93, 1–6, https://doi.org/10.1016/j.orggeochem.2015.12.006, 2016.

Huguet, C., Hopmans, E. C., Febo-Ayala, W., Thompson, D. H., Sinninghe Damsté, J. S., and Schouten, S.: An improved method to determine the absolute abundance of glycerol dibiphytanyl glycerol tetraether lipids, Org. Geochem., 37, 1036–1041, https://doi.org/10.1016/j.orggeochem.2006.05.008, 2006.

Hunt, J. B. and Hill, P. G.: An inter-laboratory comparison of the electron probe microanalysis of glass geochemistry, Quatern. Int., 34–36, 229–241, https://doi.org/10.1016/1040-6182(95)00088-7, 1996.

Jacobson, G. L. and Bradshaw, R. H. W.: The Selection of Sites for Paleovegetational Studies, Quatern. Res., 16, 80–96, https://doi.org/10.1016/0033-5894(81)90129-0, 1981.

Joannin, S., Brugiapaglia, E., de Beaulieu, J.-L., Bernardo, L., Magny, M., Peyron, O., Goring, S., and Vannière, B.: Pollen-based reconstruction of Holocene vegetation and climate in southern Italy: the case of Lago Trifoglietti, Clim. Past, 8, 1973–1996, https://doi.org/10.5194/cp-8-1973-2012, 2012.

Jochum, K. P., Stoll, B., Herwig, K., Willbold, M., Hofmann, A. W., Amini, M., Aarburg, S., Abouchami, W., Hellebrand, E., Mocek, B., Raczek, I., Stracke, A., Alard, O., Bouman, C., Becker, S., Dücking, M., Brätz, H., Klemd, R., de Bruin, D., Canil, D., Cornell, D., de Hoog, C.-J., Dalpé, C., Danyushevsky, L., Eisenhauer, A., Gao, Y., Snow, J. E., Groschopf, N., Günther, D., Latkoczy, C., Guillong, M., Hauri, E. H., Höfer, H. E., Lahaye, Y., Horz, K., Jacob, D. E., Kasemann, S. A., Kent, A. J. R., Ludwig, T., Zack, T., Mason, P. R. D., Meixner, A., Rosner, M., Misawa, K., Nash, B. P., Pfänder, J., Premo, W. R., Sun, W. D., Tiepolo, M., Vannucci, R., Vennemann, T., Wayne, D., and Woodhead, J. D.: MPI-DING reference glasses for in situ microanalysis: New reference values for element concentrations and isotope ratios: MPI-DING Refernce Glasses, Geochem. Geophy. Geosy., 7, 5–27, https://doi.org/10.1029/2005GC001060, 2006.

Juggins, S. and Juggins, M. S.: Package 'rioja', GitHub, https://github.com/nsj3/rioja (last access: 13 December 2022), 2020.

Kuehn, S. C., Froese, D. G., and Shane, P. A. R.: The INTAV intercomparison of electron-beam microanalysis of glass by tephrochronology laboratories: Results and recommendations, Quatern. Int., 246, 19–47, https://doi.org/10.1016/j.quaint.2011.08.022, 2011.

Larocque, I. and Finsinger, W.: Late-glacial chironomid-based temperature reconstructions for Lago Piccolo di Avigliana in the southwestern Alps (Italy), Palaeogeogr. Palaeocl., 257, 207–223, https://doi.org/10.1016/j.palaeo.2007.10.021, 2008.

Li, H., Spötl, C., and Cheng, H.: A high-resolution speleothem proxy record of the Late Glacial in the European Alps: extending the NALPS19 record until the beginning of the Holocene, J. Quaternary Sci., 36, 29–39, https://doi.org/10.1002/jqs.3255, 2021.

Liang, J., Russell, J. M., Xie, H., Lupien, R. L., Si, G., Wang, J., Hou, J., and Zhang, G.: Vegetation effects on temperature calibrations of branched glycerol dialkyl glycerol tetraether (brGDGTs) in soils, Org. Geochem., 127, 1–11, https://doi.org/10.1016/j.orggeochem.2018.10.010, 2019.

Liaw, A. and Wiener, M.: Classification and Regression by randomForest, https://www.stat.berkeley.edu/~breiman/RandomForests/cc_home.htm (last access: 13 December 2022), 2002.

Loomis, S. E., Russell, J. M., and Sinninghe Damsté, J. S.: Distributions of branched GDGTs in soils and lake sediments from western Uganda: Implications for a lacustrine paleothermometer, Org. Geochem., 42, 739–751, https://doi.org/10.1016/j.orggeochem.2011.06.004, 2011.

Loomis, S. E., Russell, J. M., Heureux, A. M., D'Andrea, W. J., and Sinninghe Damsté, J. S.: Seasonal variability of branched glycerol dialkyl glycerol tetraethers (brGDGTs) in a temperate lake system, Geochim. Cosmochim. Ac., 144, 173–187, https://doi.org/10.1016/j.gca.2014.08.027, 2014.

Lotter, A. F., Heiri, O., Brooks, S., van Leeuwen, J. F. N., Eicher, U., and Ammann, B.: Rapid summer temperature changes during Termination 1a: high-resolution multi-proxy climate reconstructions from Gerzensee (Switzerland), Quaternary Sci. Rev., 36, 103–113, https://doi.org/10.1016/j.quascirev.2010.06.022, 2012.

Magny, M., Combourieu-Nebout, N., de Beaulieu, J. L., Bout-Roumazeilles, V., Colombaroli, D., Desprat, S., Francke, A., Joannin, S., Ortu, E., Peyron, O., Revel, M., Sadori, L., Siani, G., Sicre, M. A., Samartin, S., Simonneau, A., Tinner, W., Vannière, B., Wagner, B., Zanchetta, G., Anselmetti, F., Brugiapaglia, E., Chapron, E., Debret, M., Desmet, M., Didier, J., Essallami, L., Galop, D., Gilli, A., Haas, J. N., Kallel, N., Millet, L., Stock, A., Turon, J. L., and Wirth, S.: North–south palaeohydrological contrasts in the central Mediterranean during the Holocene: tentative synthesis and working hypotheses, Clim. Past, 9, 2043–2071, https://doi.org/10.5194/cp-9-2043-2013, 2013.

Marchegiano, M., Horne, D. J., Gliozzi, E., Francke, A., Wagner, B., and Ariztegui, D.: Rapid Late Pleistocene climate change reconstructed from a lacustrine ostracod record in central Italy (Lake Trasimeno, Umbria), Boreas, 49, 739–750, https://doi.org/10.1111/bor.12450, 2020.

Martin, C., Ménot, G., Thouveny, N., Davtian, N., Andrieu-Ponel, V., Reille, M., and Bard, E.: Impact of human activities and vegetation changes on the tetraether sources in Lake St Front (Massif Central, France), Org. Geochem., 135, 38–52, 2019.

Martin, C., Ménot, G., Thouveny, N., Peyron, O., Andrieu-Ponel, V., Montade, V., Davtian, N., Reille, M., and Bard, E.: Early Holocene Thermal Maximum recorded by branched tetraethers and pollen in Western Europe (Massif Central, France), Quaternary Sci. Rev., 228, 106109, https://doi.org/10.1016/j.quascirev.2019.106109, 2020.

Martínez-Sosa, P., Tierney, J. E., Stefanescu, I. C., Dearing Crampton-Flood, E., Shuman, B. N., and Routson, C.: A global Bayesian temperature calibration for lacus-

trine brGDGTs, Geochim. Cosmochim. Ac., 305, 87–105, https://doi.org/10.1016/j.gca.2021.04.038, 2021.

Max, L., Lembke-Jene, L., Zou, J., Shi, X., and Tiedemann, R.: Evaluation of reconstructed sea surface temperatures based on $U37k'$ from sediment surface samples of the North Pacific, Quaternary Sci. Rev., 243, 106496, https://doi.org/10.1016/j.quascirev.2020.106496, 2020.

Mercuri, A. M., Accorsi, C. A., and Bandini Mazzanti, M.: The long history of Cannabis and its cultivation by the Romans in central Italy, shown by pollen records from Lago Albano and Lago di Nemi, Veget. Hist. Archaeobot., 11, 263–276, https://doi.org/10.1007/s003340200039, 2002.

Millet, L., Rius, D., Galop, D., Heiri, O., and Brooks, S. J.: Chironomid-based reconstruction of Lateglacial summer temperatures from the Ech palaeolake record (French western Pyrenees), Palaeogeogr. Palaeocl., 315–316, 86–99, https://doi.org/10.1016/j.palaeo.2011.11.014, 2012.

Moore, P. D., Webb, J. A., and Collinson, M. E.: Pollen Analysis, in: Subsequent edition, Blackwell Science Inc, Oxford, ISBN 10 0865428956, 13 978-0632021765, 1991.

Moreno, A., Svensson, A., Brooks, S. J., Connor, S., Engels, S., Fletcher, W., Genty, D., Heiri, O., Labuhn, I., Perşoiu, A., Peyron, O., Sadori, L., Valero-Garcés, B., Wulf, S., and Zanchetta, G.: A compilation of Western European terrestrial records 60–8 ka BP: towards an understanding of latitudinal climatic gradients, Quaternary Sci. Rev., 106, 167–185, https://doi.org/10.1016/j.quascirev.2014.06.030, 2014.

Naafs, B. D. A., Inglis, G. N., Zheng, Y., Amesbury, M. J., Biester, H., Bindler, R., Blewett, J., Burrows, M. A., del Castillo Torres, D., Chambers, F. M., Cohen, A. D., Evershed, R. P., Feakins, S. J., Gałka, M., Gallego-Sala, A., Gandois, L., Gray, D. M., Hatcher, P. G., Honorio Coronado, E. N., Hughes, P. D. M., Huguet, A., Könönen, M., Laggoun-Défarge, F., Lähteenoja, O., Lamentowicz, M., Marchant, R., McClymont, E., Pontevedra-Pombal, X., Ponton, C., Pourmand, A., Rizzuti, A. M., Rochefort, L., Schellekens, J., De Vleeschouwer, F., and Pancost, R. D.: Introducing global peat-specific temperature and pH calibrations based on brGDGT bacterial lipids, Geochim. Cosmochim. Ac., 208, 285–301, https://doi.org/10.1016/j.gca.2017.01.038, 2017a.

Naafs, B. D. A., Gallego-Sala, A. V., Inglis, G. N., and Pancost, R. D.: Refining the global branched glycerol dialkyl glycerol tetraether (brGDGT) soil temperature calibration, Org. Geochem., 106, 48–56, https://doi.org/10.1016/j.orggeochem.2017.01.009, 2017b.

Panagiotopoulos, K., Holtvoeth, J., Kouli, K., Marinova, E., Francke, A., Cvetkoska, A., Jovanovska, E., Lacey, J. H., Lyons, E. T., Buckel, C., Bertini, A., Donders, T., Just, J., Leicher, N., Leng, M. J., Melles, M., Pancost, R. D., Sadori, L., Tauber, P., Vogel, H., Wagner, B., and Wilke, T.: Insights into the evolution of the young Lake Ohrid ecosystem and vegetation succession from a southern European refugium during the Early Pleistocene, Quaternary Sci. Rev., 227, 106044, https://doi.org/10.1016/j.quascirev.2019.106044, 2020.

Peyron, O., Guiot, J., Cheddadi, R., Tarasov, P., Reille, M., de Beaulieu, J.-L., Bottema, S., and Andrieu, V.: Climatic Reconstruction in Europe for 18,000 YR B.P. from Pollen Data, Quatern. Res., 49, 183–196, https://doi.org/10.1006/qres.1997.1961, 1998.

Peyron, O., Bégeot, C., Brewer, S., Heiri, O., Magny, M., Millet, L., Ruffaldi, P., Van Campo, E., and Yu, G.: Late-Glacial climatic changes in Eastern France (Lake Lautrey) from pollen, lake-levels, and chironomids, Quatern. Res., 64, 197–211, https://doi.org/10.1016/j.yqres.2005.01.006, 2005.

Peyron, O., Goring, S., Dormoy, I., Kotthoff, U., Pross, J., de Beaulieu, J.-L., Drescher-Schneider, R., Vannière, B., and Magny, M.: Holocene seasonality changes in the central Mediterranean region reconstructed from the pollen sequences of Lake Accesa (Italy) and Tenaghi Philippon (Greece), Holocene, 21, 131–146, https://doi.org/10.1177/0959683610384162, 2011.

Peyron, O., Magny, M., Goring, S., Joannin, S., de Beaulieu, J.-L., Brugiapaglia, E., Sadori, L., Garfi, G., Kouli, K., Ioakim, C., and Combourieu-Nebout, N.: Contrasting patterns of climatic changes during the Holocene across the Italian Peninsula reconstructed from pollen data, Clim. Past, 9, 1233–1252, https://doi.org/10.5194/cp-9-1233-2013, 2013.

Peyron, O., Combourieu-Nebout, N., Brayshaw, D., Goring, S., Andrieu-Ponel, V., Desprat, S., Fletcher, W., Gambin, B., Ioakim, C., Joannin, S., Kotthoff, U., Kouli, K., Montade, V., Pross, J., Sadori, L., and Magny, M.: Precipitation changes in the Mediterranean basin during the Holocene from terrestrial and marine pollen records: a model–data comparison, Clim. Past, 13, 249–265, https://doi.org/10.5194/cp-13-249-2017, 2017.

Ponel, P., Guiter, F., Gandouin, E., Peyron, O., and de Beaulieu, J.-L.: Late-Glacial palaeotemperatures and palaeoprecipitations in the Aubrac Mountains (French Massif Central) reconstructed from multiproxy analyses (Coleoptera, chironomids and pollen), Quatern. Int., 636, 39–51, https://doi.org/10.1016/j.quaint.2022.02.005, 2022.

Prasad, A. M., Iverson, L. R., and Liaw, A.: Newer Classification and Regression Tree Techniques: Bagging and Random Forests for Ecological Prediction, Ecosystems, 9, 181–199, https://doi.org/10.1007/s10021-005-0054-1, 2006.

Prentice, C., Guiot, J., Huntley, B., Jolly, D., and Cheddadi, R.: Reconstructing biomes from palaeoecological data: a general method and its application to European pollen data at 0 and 6 ka, Clim. Dynam., 12, 185–194, https://doi.org/10.1007/BF00211617, 1996.

Raberg, J. H., Harning, D. J., Crump, S. E., de Wet, G., Blumm, A., Kopf, S., Geirsdóttir, Á., Miller, G. H., and Sepúlveda, J.: Revised fractional abundances and warm-season temperatures substantially improve brGDGT calibrations in lake sediments, Biogeosciences, 18, 3579–3603, https://doi.org/10.5194/bg-18-3579-2021, 2021.

Raberg, J. H., Flores, E., Crump, S. E., de Wet, G., Dildar, N., Miller, G. H., Geirsdóttir, Á., and Sepúlveda, J.: Intact Polar brGDGTs in Arctic Lake Catchments: Implications for Lipid Sources and Paleoclimate Applications, J. Geophys. Res.-Biogeo., 127, e2022JG006969, https://doi.org/10.1029/2022JG006969, 2022.

Ramos-Román, M. J., De Jonge, C., Magyari, E., Veres, D., Ilvonen, L., Develle, A.-L., and Seppä, H.: Lipid biomarker (brGDGT)- and pollen-based reconstruction of temperature change during the Middle to Late Holocene transition in the Carpathians, Global Planet. Change, 215, 103859, https://doi.org/10.1016/j.gloplacha.2022.103859, 2022.

Rasmussen, S. O., Bigler, M., Blockley, S. P., Blunier, T., Buchardt, S. L., Clausen, H. B., Cvijanovic, I., Dahl-Jensen, D., Johnsen, S.

J., Fischer, H., Gkinis, V., Guillevic, M., Hoek, W. Z., Lowe, J. J., Pedro, J. B., Popp, T., Seierstad, I. K., Steffensen, J. P., Svensson, A. M., Vallelonga, P., Vinther, B. M., Walker, M. J. C., Wheatley, J. J., and Winstrup, M.: A stratigraphic framework for abrupt climatic changes during the Last Glacial period based on three synchronized Greenland ice-core records: refining and extending the INTIMATE event stratigraphy, Quaternary Sci. Rev., 106, 14–28, https://doi.org/10.1016/j.quascirev.2014.09.007, 2014.

Rea, B. R., Pellitero, R., Spagnolo, M., Hughes, P., Ivy-Ochs, S., Renssen, H., Ribolini, A., Bakke, J., Lukas, S., and Braithwaite, R. J.: Atmospheric circulation over Europe during the Younger Dryas, Sci. Adv., 6, eaba4844, https://doi.org/10.1126/sciadv.aba4844, 2020.

Regattieri, E., Zanchetta, G., Drysdale, R. N., Isola, I., Hellstrom, J. C., and Dallai, L.: Lateglacial to Holocene trace element record (Ba, Mg, Sr) from Corchia Cave (Apuan Alps, central Italy): paleoenvironmental implications: Trace element record from Corchia Cave, central Italy, J. Quaternary Sci., 29, 381–392, https://doi.org/10.1002/jqs.2712, 2014.

Rehfeld, K., Münch, T., Ho, S. L., and Laepple, T.: Global patterns of declining temperature variability from the Last Glacial Maximum to the Holocene, Nature, 554, 356–359, https://doi.org/10.1038/nature25454, 2018.

Reille, M.: Pollen et spores d'Europe et d'Afrique du Nord, Supplément 1, in: Éditions du Laboratoire de botanique historique et palynologie, Laboratoire de botanique historique et palynologie, Marseille, p. 327, ISBN 13 978-2-9507175-4-2, 1998.

Reille, M.: Pollen et spores d'Europe et d'Afrique du Nord, Supplément 2 in: Éditions du Laboratoire de botanique historique et palynologie, Laboratoire de botanique historique et palynologie, Marseille, p. 530, https://doi.org/10.7202/004885ar, 1998.

Reimer, P. J., Austin, W. E. N., Bard, E., Bayliss, A., Blackwell, P. G., Ramsey, C. B., Butzin, M., Cheng, H., Edwards, R. L., Friedrich, M., Grootes, P. M., Guilderson, T. P., Hajdas, I., Heaton, T. J., Hogg, A. G., Hughen, K. A., Kromer, B., Manning, S. W., Muscheler, R., Palmer, J. G., Pearson, C., Plicht, J. van der, Reimer, R. W., Richards, D. A., Scott, E. M., Southon, J. R., Turney, C. S. M., Wacker, L., Adolphi, F., Büntgen, U., Capano, M., Fahrni, S. M., Fogtmann-Schulz, A., Friedrich, R., Köhler, P., Kudsk, S., Miyake, F., Olsen, J., Reinig, F., Sakamoto, M., Sookdeo, A., and Talamo, S.: The IntCal20 Northern Hemisphere Radiocarbon Age Calibration Curve (0–55 cal kBP), Radiocarbon, 62, 725–757, https://doi.org/10.1017/RDC.2020.41, 2020.

Renssen, H. and Isarin, R. F. B.: The two major warming phases of the last deglaciation at ∼ 14.7 and ∼ 11.5 ka cal BP in Europe: climate reconstructions and AGCM experiments, Global Planet. Change, 30, 117–153, https://doi.org/10.1016/S0921-8181(01)00082-0, 2001.

Renssen, H., Mairesse, A., Goosse, H., Mathiot, P., Heiri, O., Roche, D. M., Nisancioglu, K. H., and Valdes, P. J.: Multiple causes of the Younger Dryas cold period, Nat. Geosci., 8, 946–949, https://doi.org/10.1038/ngeo2557, 2015.

Robles, M.: Vegetation, climate, and human history of the Mediterranean basin: A Late-Glacial to Holocene reconstruction from Italy (Lake Matese) to Armenia (Lake Sevan) inferred from a multi-proxy approach (pollen, NPPs, brGDGTs, XRF), PhD thesis, University of Molise, University of Montpellier, Campobasso, Montpellier, https://www.theses.fr/s217687, last access: 13 December 2022.

Robles, M., Peyron, O., Brugiapaglia, E., Ménot, G., Dugerdil, L., Ollivier, V., Ansanay-Alex, S., Develle, A.-L., Tozalakyan, P., Meliksetian, K., Sahakyan, K., Sahakyan, L., Perello, B., Badalyan, R., Colombié, C., and Joannin, S.: Impact of climate changes on vegetation and human societies during the Holocene in the South Caucasus (Vanevan, Armenia): A multiproxy approach including pollen, NPPs and brGDGTs, Quaternary Sci. Rev., 277, 107297, https://doi.org/10.1016/j.quascirev.2021.107297, 2022.

Rodrigo-Gámiz, M., García-Alix, A., Jiménez-Moreno, G., Ramos-Román, M. J., Camuera, J., Toney, J. L., Sachse, D., Anderson, R. S., and Sinninghe Damsté, J. S.: Paleoclimate reconstruction of the last 36 kyr based on branched glycerol dialkyl glycerol tetraethers in the Padul palaeolake record (Sierra Nevada, southern Iberian Peninsula), Quaternary Sci. Rev., 281, 107434, https://doi.org/10.1016/j.quascirev.2022.107434, 2022.

Russell, J. M., Hopmans, E. C., Loomis, S. E., Liang, J., and Sinninghe Damsté, J. S.: Distributions of 5- and 6-methyl branched glycerol dialkyl glycerol tetraethers (brGDGTs) in East African lake sediment: Effects of temperature, pH, and new lacustrine paleotemperature calibrations, Org. Geochem., 117, 56–69, https://doi.org/10.1016/j.orggeochem.2017.12.003, 2018.

Sadori, L.: The Lateglacial and Holocene vegetation and climate history of Lago di Mezzano (central Italy), Quaternary Sci. Rev., 202, 30–44, https://doi.org/10.1016/j.quascirev.2018.09.004, 2018.

Salonen, J. S., Korpela, M., Williams, J. W., and Luoto, M.: Machine-learning based reconstructions of primary and secondary climate variables from North American and European fossil pollen data, Sci. Rep., 9, 15805, https://doi.org/10.1038/s41598-019-52293-4, 2019.

Samartin, S., Heiri, O., Joos, F., Renssen, H., Franke, J., Brönnimann, S., and Tinner, W.: Warm Mediterranean mid-Holocene summers inferred from fossil midge assemblages, Nat. Geosci., 10, 207–212, https://doi.org/10.1038/ngeo2891, 2017.

Sanchi, L., Ménot, G., and Bard, E.: Insights into continental temperatures in the northwestern Black Sea area during the Last Glacial period using branched tetraether lipids, Quaternary Sci. Rev., 84, 98–108, https://doi.org/10.1016/j.quascirev.2013.11.013, 2014.

Sbaffi, L., Wezel, F. C., Curzi, G., and Zoppi, U.: Millennial- to centennial-scale palaeoclimatic variations during Termination I and the Holocene in the central Mediterranean Sea, Global Planet. Change, 40, 201–217, https://doi.org/10.1016/S0921-8181(03)00111-5, 2004.

Sicre, M.-A., Siani, G., Genty, D., Kallel, N., and Essallami, L.: Seemingly divergent sea surface temperature proxy records in the central Mediterranean during the last deglacial, Clim. Past, 9, 1375–1383, https://doi.org/10.5194/cpd-9-683-2013, 2013.

Sinninghe Damsté, J. S., Rijpstra, W. I. C., Foesel, B. U., Huber, K. J., Overmann, J., Nakagawa, S., Kim, J. J., Dunfield, P. F., Dedysh, S. N., and Villanueva, L.: An overview of the occurrence of ether- and ester-linked iso-diabolic acid membrane lipids in microbial cultures of the Acidobacteria: Implications for brGDGT paleoproxies for temperature and pH, Org. Geochem., 124, 63–76, https://doi.org/10.1016/j.orggeochem.2018.07.006, 2018.

Smith, V. C., Isaia, R., and Pearce, N. J. G.: Tephrostratigraphy and glass compositions of post-15 kyr Campi Fle-

grei eruptions: implications for eruption history and chronostratigraphic markers, Quaternary Sci. Rev., 30, 3638–3660, https://doi.org/10.1016/j.quascirev.2011.07.012, 2011.

Stockhecke, M., Bechtel, A., Peterse, F., Guillemot, T., and Schubert, C. J.: Temperature, precipitation, and vegetation changes in the Eastern Mediterranean over the last deglaciation and Dansgaard-Oeschger events, Palaeogeogr. Palaeocl., 577, 110535, https://doi.org/10.1016/j.palaeo.2021.110535, 2021.

Sun, Q., Chu, G., Liu, M., Xie, M., Li, S., Ling, Y., Wang, X., Shi, L., Jia, G., and Lü, H.: Distributions and temperature dependence of branched glycerol dialkyl glycerol tetraethers in recent lacustrine sediments from China and Nepal, J. Geophys. Res., 116, G01008, https://doi.org/10.1029/2010JG001365, 2011.

Taffetani, F., Catorci, A., Ciaschetti, G., Cutini, M., Di Martino, L., Frattaroli, A. R., Paura, B., Pirone, G., Rismondo, M., and Zitti, S.: The Quercus cerris woods of the alliance Carpinion orientalis Horvat 1958 in Italy, Plant Biosyst., 146, 918–953, https://doi.org/10.1080/11263504.2012.682613, 2012.

Tarroso, P., Carrión, J., Dorado-Valiño, M., Queiroz, P., Santos, L., Valdeolmillos-Rodríguez, A., Célio Alves, P., Brito, J. C., and Cheddadi, R.: Spatial climate dynamics in the Iberian Peninsula since 15 000 yr BP, Clim. Past, 12, 1137–1149, https://doi.org/10.5194/cp-12-1137-2016, 2016.

ter Braak, C. J. F. and Juggins, S.: Weighted averaging partial least squares regression (WA-PLS): an improved method for reconstructing environmental variables from species assemblages, Hydrobiologia, 269/270, 485–502, 1993.

ter Braak, C. J. F. and van Dam, H.: Inferring pH from diatoms: a comparison of old and new calibration methods, Hydrobiologia, 178, 209–223, https://doi.org/10.1007/BF00006028, 1989.

Tomlinson, E. L., Arienzo, I., Civetta, L., Wulf, S., Smith, V. C., Hardiman, M., Lane, C. S., Carandente, A., Orsi, G., Rosi, M., Müller, W., and Menzies, M. A.: Geochemistry of the Phlegraean Fields (Italy) proximal sources for major Mediterranean tephras: Implications for the dispersal of Plinian and co-ignimbritic components of explosive eruptions, Geochim. Cosmochim. Ac., 93, 102–128, https://doi.org/10.1016/j.gca.2012.05.043, 2012.

Valente, E., Buscher, J. T., Jourdan, F., Petrosino, P., Reddy, S. M., Tavani, S., Corradetti, A., and Ascione, A.: Constraining mountain front tectonic activity in extensional setting from geomorphology and Quaternary stratigraphy: A case study from the Matese ridge, southern Apennines, Quaternary Sci. Rev., 219, 47–67, https://doi.org/10.1016/j.quascirev.2019.07.001, 2019.

Van Geel, B.: Non-Pollen Palynomorphs, in: Tracking Environmental Change Using Lake Sediments, vol. 3, edited by: Smol, J. P., Birks, H. J. B., Last, W. M., Bradley, R. S., and Alverson, K., Springer Netherlands, Dordrecht, 99–119, https://doi.org/10.1007/0-306-47668-1_6, 2002.

Vescovi, E., Kaltenrieder, P., and Tinner, W.: Late-Glacial and Holocene vegetation history of Pavullo nel Frignano (Northern Apennines, Italy), Rev. Palaeobot. Palynol., 160, 32–45, https://doi.org/10.1016/j.revpalbo.2010.01.002, 2010.

Walker, M., Lowe, J., Blockley, S. P. E., Bryant, C., Coombes, P., Davies, S., Hardiman, M., Turney, C. S. M., and Watson, J.: Lateglacial and early Holocene palaeoenvironmental 'events' in Sluggan Bog, Northern Ireland: comparisons with the Greenland NGRIP GICC05 event stratigraphy, Quaternary Sci. Rev., 36, 124–138, https://doi.org/10.1016/j.quascirev.2011.09.008, 2012.

Watson, B. I., Williams, J. W., Russell, J. M., Jackson, S. T., Shane, L., and Lowell, T. V.: Temperature variations in the southern Great Lakes during the last deglaciation: Comparison between pollen and GDGT proxies, Quaternary Sci. Rev., 182, 78–92, https://doi.org/10.1016/j.quascirev.2017.12.011, 2018.

Weijers, J. W. H., Schouten, S., Spaargaren, O. C., and Sinninghe Damsté, J. S.: Occurrence and distribution of tetraether membrane lipids in soils: Implications for the use of the TEX86 proxy and the BIT index, Org. Geochem., 37, 1680–1693, https://doi.org/10.1016/j.orggeochem.2006.07.018, 2006.

Weijers, J. W. H., Schouten, S., van den Donker, J. C., Hopmans, E. C., and Sinninghe Damsté, J. S.: Environmental controls on bacterial tetraether membrane lipid distribution in soils, Geochim. Cosmochim. Ac., 71, 703–713, https://doi.org/10.1016/j.gca.2006.10.003, 2007.

Weijers, J. W. H., Panoto, E., van Bleijswijk, J., Schouten, S., Rijpstra, W. I. C., Balk, M., Stams, A. J. M., and Damsté, J. S. S.: Constraints on the Biological Source(s) of the Orphan Branched Tetraether Membrane Lipids, Geomicrobiol. J., 26, 402–414, https://doi.org/10.1080/01490450902937293, 2009.

Wulf, S., Kraml, M., Brauer, A., Keller, J., and Negendank, J. F. W.: Tephrochronology of the 100 ka lacustrine sediment record of Lago Grande di Monticchio (southern Italy), Quatern. Int., 122, 7–30, https://doi.org/10.1016/j.quaint.2004.01.028, 2004.

Wulf, S., Kraml, M., and Keller, J.: Towards a detailed distal tephrostratigraphy in the Central Mediterranean: The last 20,000 yrs record of Lago Grande di Monticchio, J. Volcanol. Geoth. Res., 177, 118–132, https://doi.org/10.1016/j.jvolgeores.2007.10.009, 2008.

Yang, H., Pancost, R. D., Dang, X., Zhou, X., Evershed, R. P., Xiao, G., Tang, C., Gao, L., Guo, Z., and Xie, S.: Correlations between microbial tetraether lipids and environmental variables in Chinese soils: Optimizing the paleo-reconstructions in semi-arid and arid regions, Geochim. Cosmochim. Ac., 126, 49–69, https://doi.org/10.1016/j.gca.2013.10.041, 2014.

Zhang, J., Bai, Y., Xu, S., Lei, F., and Jia, G.: Alkenone and tetraether lipids reflect different seasonal seawater temperatures in the coastal northern South China Sea, Org. Geochem., 58, 115–120, https://doi.org/10.1016/j.orggeochem.2013.02.012, 2013.